THE MANE PROCESS OF GENERATING CONTINUOUS ENERGY HOT-OPERATING TEMPERATURE CROSS SECTIONS

A Thesis
Presented to
The Academic Faculty

by

Christopher Weeks Chapman

In Partial Fulfillment
of the Requirements for the Degree
Master of Science in Nuclear Engineering in the
Nuclear and Radiological Engineering and Medical Physics Program,
George W. Woodruff School of Mechanical Engineering

Georgia Institute of Technology
December 2014

THE MANE PROCESS OF GENERATING CONTINUOUS ENERGY

HOT-OPERATING TEMPERATURE CROSS SECTIONS

Approved by:

Dr. Farzad Rahnema, Advisor
School of Mechanical Engineering
Georgia Institute of Technology

Dr. Bojan Petrovic
School of Mechanical Engineering
Georgia Institute of Technology

Dr. Dingkang Zhang
School of Mechanical Engineering
Georgia Institute of Technology

Date Approved: June 12, 2014

ACKNOWLEDGEMENTS

I would like to thank my advisor Dr. Farzad Rahnema for his guidance as well as Dr. Dingkang Zhang and Dr. Bojan Petrovic for serving on my committee. I would also like to acknowledge that this research is being performed using funding received from the DOE Office of Nuclear Energy's Nuclear Energy University Programs

TABLE OF CONTENTS

LIST OF TABLES

LIST OF FIGURES

SUMMARY

MANE (MCNP ACE from NJOY & ENDF), a code for generating continuous energy cross sections at arbitrary temperatures, was created. Cross sections were evaluated using NJOY99 such that they would agree with the cross sections provided by MCNP5. The MANE cross sections were found to be in very good agreement with those provided by MCNP5 with some minor exceptions caused by round-off errors and some differences in the unresolved resonance region. Differences in the resonance region are caused by differences in the random number generator used to start the cross section calculations. The MANE cross sections were verified against the MCNP5 cross sections in five unique MCNP configurations: an 8.7% enriched MOX fuel pin cell, a UO_2 assembly (controlled and uncontrolled), a MOX assembly, and a whole core configuration containing the 3 assemblies. In each of these cases, eigenvalue and tally density results were found to be in very good agreement with one another.

CHAPTER 1

INTRODUCTION

With the increase of transport equation solvers, there is a need for whole-core, hot-operating temperature computational transport benchmark problems for verification and numerical benchmarking. One of the main issues with evaluating these benchmarks is generating the cross sections necessary for the problems. Currently, these cross sections are generated using transport lattice depletion codes resulting in multi-group approximated cross sections. There are some issues with this method of cross section generation. Multi-group cross sections are flux-weighted on an assembly level, and often do not take core environment effects into consideration. The cross sections are also often spatially homogenized, further neglecting core environment effects. One solution to this problem is to use continuous energy cross sections thereby avoiding the multigroup approximation entirely.

Generating continuous energy hot-operating temperatures is traditionally done by a post-processing nuclear data code such as NJOY [1]. NJOY is the post-processing code used by the Monte Carlo code MCNP [2] to generate its continuous-energy cross sections. The disadvantage of these cross sections is they are only provided at particular temperature values. In order to generate cross sections at a different temperature, one must either re-evaluate the cross sections from the ENDF files or use the MAKXSF [3] utility code provided by MCNP. This utility code does not interpolate temperatures for thermal scattering cross sections and only changes cross sections already provided by MCNP.

The MANE (MCNP ACE from NJOY and ENDF) code is a utility code that generates the ACE format cross sections at arbitrary temperatures from any ENDF6 format cross section file such that they match the cross sections provided by MCNP. It can also generate temperature-dependent $S(\alpha,\beta)$ files required for thermal scattering files.

To verify the cross section generation process, MANE generated cross sectiosn were compared to the ENDF/B-VII cross section libraries provided with the MCNP5 code. This was done to show that any differences are due to machine-dependent issues (round-off errors or errors associated with random number generators). As an additional measure, various eigenvalue and tally-density distributions were generated using MCNP5. To show this, five cases were considered: an 8.7% MOX fuel pin, a UO_2 assembly (with and without control rods), a MOX assembly, and a whole-core configuration (comprised of the UO_2 and MOX assemblies).

An overview of MANE and the comparison between the cross section it produces and those from the MCNP library are found in Chapter 2. A more detailed description of the geometries and material properties of the cases described above are in Chapter 3. Details and analysis of the comparison MCNP runs are in Chapter 4. Concluding remarks and potential areas of future work are discussed in Chapter 5.

CHAPTER 2

MANE

The MCNP ACE from NJOY & ENDF (MANE) code easily allows users to create continuous energy cross sections for use in MCNP5/MCNPX by using NJOY99.248 to evaluate ENDF cross sections. Based off of the user inputs and ENDF files provided, MANE will create the necessary NJOY input decks and run NJOY using those input decks. MANE then saves the ACE formatted files while automatically updating the xsdir file required for MCNP to properly run. MANE can generate two kinds of cross section files: fast data and thermal data. Here, fast data will mean all of the cross sections that are not explicitly thermal scattering files, and thermal data will refer to the thermal scattering files. In the case of thermal scattering files, MANE will create the S(α,β) files required for the thermal scattering treatment.

Description of MANE

The NJOY modules utilized by MANE are the MODER, RECONR, BROADR, HEATR, PURR, LEAPR, THERMR, and GASPR modules. A more detailed description of the modules can be found in the NJOY manual [4], but a brief description of the modules is given below.

- NJOY directs the flow of data through the other modules. Subsidiary modules for locale, ENDF formats, physics constants, utility routines, and math routines are grouped with the NJOY module for descriptive purposes.
- MODER converts ENDF "tapes" back and forth between formatted (that is, ASCII) and blocked binary modes.
- RECONR reconstructs pointwise (energy-dependent) cross sections from ENDF resonance parameters and interpolation schemes.
- BROADR Doppler-broadens and thins pointwise cross sections.

- HEATR generates pointwise heat production cross sections (neutron KERMA factors) and radiation damage production cross sections.
- PURR is used to prepare unresolved-region probability tables for the MCNP continuous-energy Monte Carlo code.
- LEAPR produces thermal scattering data in ENDF-6 File 7 format that can be processed using the THERMR module.
- THERMR produces cross sections and energy-to-energy matrices for free or bound scatterers in the thermal energy range.
- GASPR generates gas-production cross sections in the pointwise PENDF format from basic ENDF cross sections.
- ACER prepares libraries in ACE format for the Los Alamos continuous-energy Monte Carlo MCNP and MCNPX codes. The ACER module is supported by subsidiary modules for the different classes of the ACE format.

In the case of a fast data input, all of the above subroutines are utilized with the exception of the LEAPR module. The input deck is constructed to match the input deck used to generate the cross sections used in MCNP [5]. Then NJOY is run for this first input, which calls on all of the modules except for ACER. After this, MANE loops through building a second input file for each individual temperature evaluation, only calls MODER and ACER. MANE then adds the corresponding xsdir information needed for MCNP use to an already existing xsdir file. This is repeated for each continuous energy nuclide input.

When thermal data input is called, the first NJOY input calls the LEAPR subroutine as well as the NJOY subroutines listed above. The input deck is again constructed to match the input deck used to generate the cross sections used in MCNP [ENDF70SAB]. In the LEAPR subroutine, MANE copies the same LEAPR inputs that were used to generate the ENDF thermal scattering files [4, 6, 7, 8]. It builds the S(α,β) file from the frequency distribution, oscillator weights, and energy weights over a

specified α and β grid in the LEAPR inputs for one temperature, and extrapolate to other temperatures from there.

The exception is Hydrogen in H_2O, which gives frequency distributions, oscillator weights, and energy weights for several different temperatures. Because of this, if Hydrogen in H_2O is evaluated, MANE performs a linear interpolation over the various input parameters required for the LEAPR input (frequency distribution, oscillator weights, and energy weights). If the temperature is above the maximum temperature given in the LEAPR input, the parameters of the maximum temperature are used.

Comparison of Cross Sections

To show MANE gives cross sections similar to those provided by MCNP, several cross sections at temperatures matching those found in MCNP's cross sections were evaluated. These cross sections are, in turn, used for the MANE validation runs discussed in the following chapter. The cross section and corresponding temperatures at which they were evaluated are shown in Appendix A.

In the all of the cross section files, there were very few differences outside of the unresolved resonance regions. The reason for the similarities comes from the fact the template used to run NJOY was the same used to generate the MCNP cross sections [5]. The same version of NJOY (NJOY99.248) was used as well. In order to agree with the MCNP cross sections better, some of the ENDF7 files had to be manually changed, as outlined in the LANL memo [5]. The only major difference was occasionally the MCNP cross section files would contain 1 additional energy point and corresponding cross sections. There were several places where the cross sections differed between the two files, but they were on the order of 10^{-6}, which can be attributed to machine precision differences.

The differences in the unresolved resonance regions, which only appear in the fast data, come from the unresolved-range probability tables calculated by the PURR

subroutine of NJOY. PURR calls a random number to start the probability table calculations, and this initial random number is different between MCNP's cross sections and MANE's cross sections. In order to better categorize these differences, the probability tables between the two cross section sets were compared. A table of 20 probability bins and corresponding cross sections is calculated for each incident neutron energy. The cross sections calculated are total, elastic scattering, fission, capture, and heating. A probability distribution for each of these cross sections is calculated, which contains a probability bin and a corresponding cross section. From these distributions, the Bondarenko cross section can be calculated as a means of comparing the two distribution sets using equation 1 below

$$\sigma_x(E) = \frac{\sum_i \frac{P_i(E)\sigma_{xi}(E)}{\sigma_0 + \sigma_{ti}(E)}}{\sum_i \frac{P_i(E)}{\sigma_0 + \sigma_{ti}(E)}} \quad (1)$$

where $\sigma_x(E)$ is the cross section of interest, $P_i(E)$ is the probability found in bin i, $\sigma_{xi}(E)$ is the cross section of interest found in probability bin i, and σ_0 is the sigma zero value, which is an input parameter for the PURR subroutine. A table of the nuclides with the percent difference between the two calculated Bondarenko cross sections and standard deviation between MCNP and MANE's values is shown on the following page in Table 1. Select cross sections and temperatures were chosen to give a representative idea of what sorts of trends can be seen from the comparison.

Based on the results in Table 1, increasing the incident energy does not appear to have any sort of significant effect on the percent error, nor did increasing the temperature. It is important to note that, while the average and standard deviations of these cross sections appear good, the actual distributions can vary drastically.

Table 1: Unresolved range probability table comparison

Nuclide	Temperature (K)	Incident Energy (keV)	Cross Section	MANE AVG & S.D.	MCNP AVG & S.D.
Zr-91	600	5.00E+01	Capture	4.05E-02 (5.98E-02)	4.05E-02 (5.92E-02)
	900	7.00E+01	Total	8.93E+00 (8.25E+00)	8.93E+00 (8.58E+00)
Zr-92	600	7.10E+01	Total	8.85E+00 (2.00E+01)	8.85E+00 (1.88E+01)
	900	1.00E+02	Elastic	9.13E+00 (1.50E+01)	9.13E+00 (1.46E+01)
Zr-94	600	1.00E+02	Heating	1.94E-03 (4.20E-06)	1.94E-03 (3.68E-06)
	900	9.00E+01	Capture	1.90E-02 (2.37E-02)	1.90E-02 (2.30E-02)
U-235	600	2.50E+00	Fission	5.34E+00 (2.49E+00)	5.34E+00 (2.43E+00)
	1200	1.31E+01	Elastic	1.16E+00 (3.28E-02)	1.16E+00 (3.11E-02)
U-238	1200	3.00E+01	Total	1.38E+01 (3.70E+00)	1.38E+01 (3.31E+00)
	1200	8.00E+01	Heating	1.00E+00 (5.06E-02)	1.00E+00 (5.04E-02)
Pu-238	1200	6.30E-01	Fission	2.76E+00 (6.19E+00)	2.76E+00 (5.96E+00)
	1200	8.00E+00	Capture	1.68E+00 (4.12E-01)	1.68E+00 (4.44E-01)
Pu-239	1200	2.85E+00	Total	1.94E+01 (6.65E+00)	1.94E+01 (8.04E+00)
	1200	4.38E+00	Fission	2.51E+00 (1.37E+00)	2.51E+00 (1.04E+00)
Pu-240	1200	2.50E+01	Heating	1.26e+00 (1.32e-01)	1.26e+00 (1.32e-01)
	1200	4.00E+01	Capture	6.31e-01 (9.67e-02)	6.31e-01 (9.51e-02)
Pu-241	1200	3.00E-01	Fission	2.15e+01 (2.38e+01)	2.15e+01 (2.38e+01)
	1200	9.50E-01	Total	2.49e+01 (1.13e+01)	2.49e+01 (1.13e+01)
Pu-242	1200	9.86E-01	Elastic	1.87e+01 (4.65e+01)	1.87e+01 (4.49e+01)
	1200	1.00E+01	Heating	2.52e-01 (6.23e-02)	2.52e-01 (6.63e-02)
Am-241	1200	4.50E-01	Fission	1.08e-01 (5.69e-02)	1.08e-01 (5.51e-02)
	1200	3.50E+00	Capture	5.91e+00 (1.48e+00)	5.91e+00 (1.62e+00)

While these differences can appear to be large in magnitude, they only account for a fraction of the energies of the cross section file. For example, the isotope with the largest number of tables (Pu-239) had tables for 70 incident energies, but had a total of 49,091 energies, which is less than 0.2% of the total number of energies. Even with the discrepancies in these probability tables, they should not lead to large errors in the MCNP evaluations.

CHAPTER 3

BENCHMARKING MANE

While the cross sections themselves agree very well as seen in the previous chapter, it is desired to show the results obtained by running MCNP with them are good as well. To show this, five cases are considered: an 8.7% MOX fuel pin, a UO_2 assembly (with and without control rods), a MOX assembly, and a whole-core configuration. The parameters and material specifications were taken from the benchmark by Rahnema and Hon [9], and are summarized here.

Each pin cell is 1.26 cm in width and filled with moderating material. A cylindrical fuel rod, surrounded by zirconium cladding, is centered in each pin cell. For the pin cell case, an 8.7% by weight trans-uranic (TRU) enriched MOX fuel pin was used. The two assemblies investigated are UO_2 and MOX. There are two control states for the UO_2 assembly: a controlled and uncontrolled case. Guide tubes are modeled so there is an interior cylinder of moderating material surrounded by an annular cylinder of zirconium cladding. The control rods contain a cylinder of control material, surrounded by a cylinder of zirconium. A gap of moderator material separates the inner zirconium from the outer zirconium clad. Each assembly is a 17x17 square lattice of pin cells with 24 guide tubes (or control rods) evenly spaced throughout and one central guide tube. A schematic is shown below in figure 1

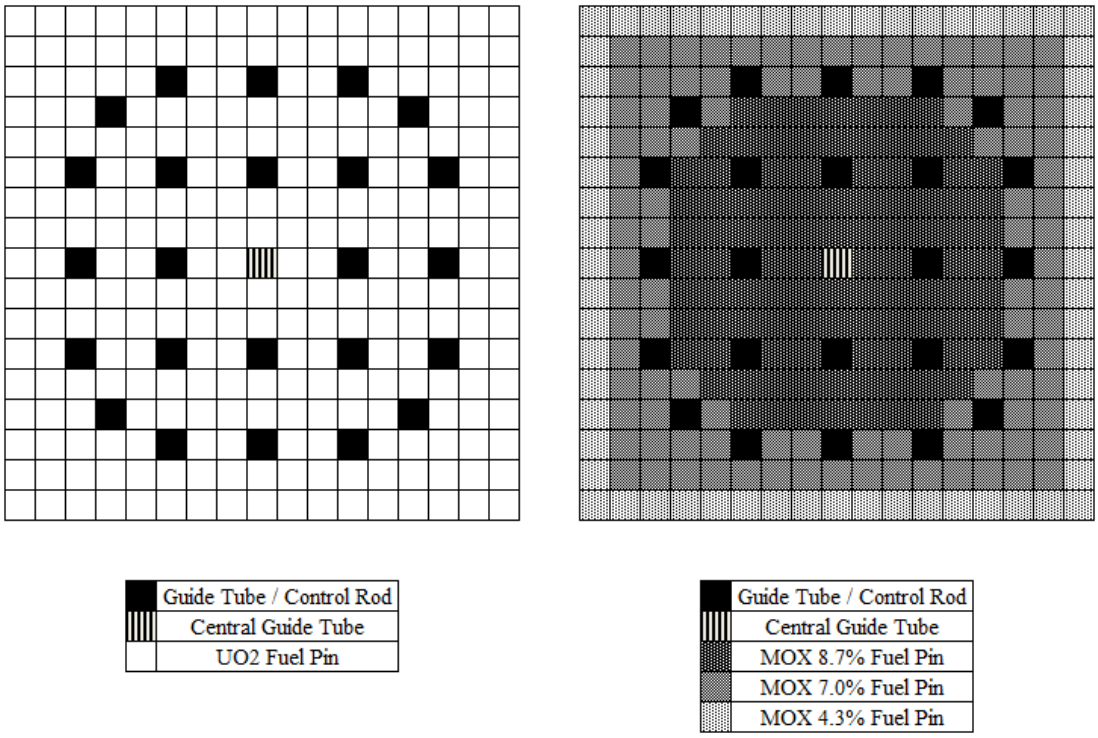

Figure 1: PWR fuel assemblies (UO_2 left, MOX right) [9]

All of the fuel rods in the UO_2 assembly have the same enrichment, while the MOX assembly has fuel rods with three unique transuranic (TRU) enrichments of 8.7%, 7.0%, and 4.3% by weight TRU. The controlled UO_2 assembly has control rods in the guide tube locations. Some assembly parameters are shown in Table 2. The isotopic composition of each material is shown in Appendix B.

Table 2: Fuel assembly parameters

Number of Fuel Pins	264
Number of Control Rods / Guide Tubes	24
Fuel Pin Radius (cm)	0.4095
Fuel Pin Clad Radius (cm)	0.54
Control Radius (cm)	0.4331
Guide Tube Inner Radius (cm)	0.573
Guide Tube / Control Rod Outer Radius (cm)	0.613
Pin Pitch (cm)	1.26
Fuel Temperature (K)	900
Structure Temperature (K)	600
Moderator Temperature (K)	576

The whole core runs are based on the some rods in (SRI) configuration from the benchmark. The whole core layout is simplified by assuming $1/8^{th}$ symmetry, as shown below in figure 2. The axial layout is comprised of 7 layers: a top plug, tube/spring, 4 core layers, and a bottom plug. The SRI configuration has several control rods partially inserted throughout the core. For the purposes of the verification runs, I will be analyzing 4 assemblies from the third core layer from the bottom (the middle assemblies in the core): assemblies 2, 3, 9, and 11 (MOX, uncontrolled UO2, MOX, and controlled UO_2, respectively).

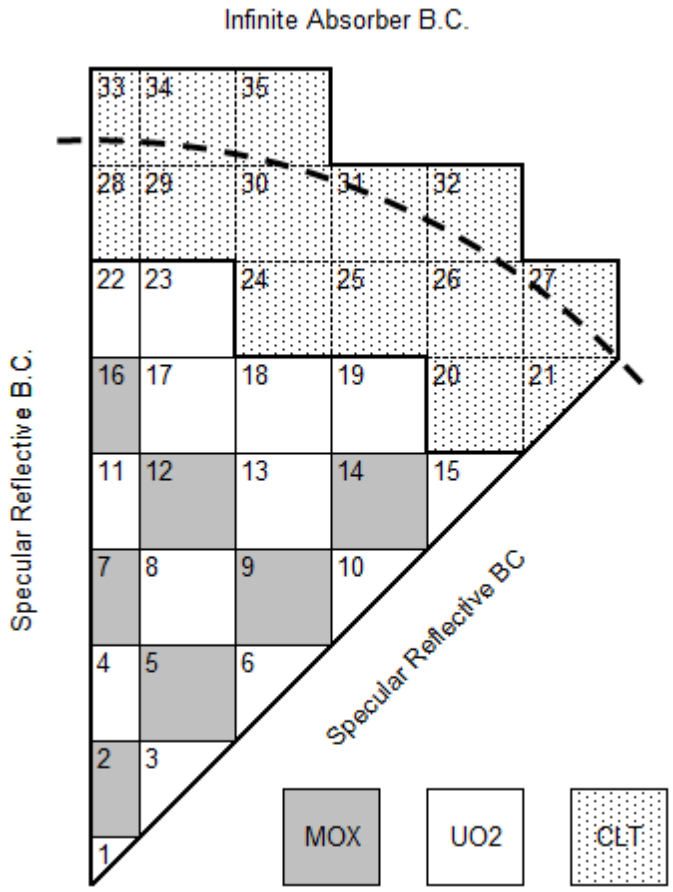

Figure 2: 1/8th symmetry whole core layout with assembly indices; the dashed line represents the core barrel. [9]

CHAPTER 4

VERIFICATION RESULTS

For each of the five cases, the source was first converged using the MCNP cross sections with 6000 cycles of 250,000 histories per cycle. This total of 1.5 billion particles was used so the statistics would be sufficient for this verification run. This source was then used for both the MCNP cross section run and MANE cross section run. Both runs used 6000 cycles (rejecting the first 400) of 250,000 histories per cycle.

Pin Cell

The results of the pin-cell eigenvalue are shown below in Table 3. The difference of 2 pcm is due to the statistical nature of MCNP and not due to the differences in the cross sections.

Table 3: 8.7% MOX pin cell eigenvalue results

Cross Section Set	MCNP	MANE
k_∞	1.03700	1.03702
Standard Deviation (pcm)	2	2
Difference (pcm)	-	2

In addition to the eigenvalue, the flux in the fuel region, clad, and moderator region were tallied as well as the fission density in the fuel region. These were tallied over 47 and 190 energy groups. For all 8 of these tallies, the percent error between the MCNP and MANE results were calculated using equation 2 below

$$p_g = \frac{\left| X^g_{mane} - X^g_{mcnp} \right|}{X^g_{mcnp}} \qquad (2)$$

where p_g is the g-group percent error, X^g_{mane} is the g-group tally from the MANE run, and X^g_{mcnp} is the g-group tally from the MCNP run. The root mean square error (RMS) and the mean relative error (MRE) are also calculated using equations 3 and 4 below

$$RME = \sqrt{\frac{\sum_g \left(\frac{X^g_{mane} - X^g_{mcnp}}{X^g_{mcnp}} \right)^2}{G}} \tag{3}$$

$$MRE = \frac{\sum_g \left(p_g * X^g_{mane} \right)}{\sum_g X^g_{mcnp}} \tag{4}$$

where G is the total number of groups being summed over (either 47 or 190 depending on the tally). The average percent error (AVG), maximum percent error (MAX), RMS percent error and MRE percent error are shown below in Table 4.

Table 4: 8.7% MOX pin cell tally results

Material	Tally	Energy group	MAX & S.D. (%)	AVG (%)	RMS (%)	MRE (%)
Fuel	Flux	47	9.970 (12.127)	0.223	1.439	0.010
		190	9.970 (12.127)	0.103	0.766	0.017
	Fission Density	47	6.798 (11.446)	0.156	0.981	0.012
		190	6.798 (11.446)	0.092	0.593	0.021
Clad	Flux	47	3.370 (9.261)	0.086	0.487	0.013
		190	4.116 (3.740)	0.072	0.391	0.020
Water	Flux	47	2.291 (2.445)	0.061	0.331	0.012
		190	2.291 (2.445)	0.040	0.175	0.019

For each of the tallies, the maximum percent error occurred at the lowest energy groups (.0001 eV-.0124 eV), where the uncertainty is on the order of 10% (with the exception of the tallies in the moderator, where the uncertainties are on the order of 1%). This explains why the RMS is significantly larger than the AVG as shown above in Table

3. The MRE is less than the other two percentages because the MRE is weighted towards the maximum value of the flux, which occurs in regions where the tallies are in good agreement. The primary source of the differences in the fuel and cladding material come from the differences in the unresolved probability tables. Even with those differences, the percent error is within the statistical uncertainties of MCNP. The results are much better in the moderator because the cross sections there are identical (with the exception of some round-off errors mentioned earlier). The significantly smaller differences in the moderator are due to the fact that the cross sections there are identical (minus some round-off errors as mentioned earlier)

Figures 3-10 are the graphical results of the energy-dependent tally in the pin cell. In each of the plots, the tallies were normalized using equation 5 below

$$X_{new}^{g} = \frac{X_{old}^{g}}{\sum_{g} X_{old}^{g} * \left(E_g - E_{g-1}\right)} \tag{5}$$

where X_{old}^{g} is the un-normalized tally in group g, and E_g is the energy in group g. Plots of these normalized tallies, along with the percent error between the two tallies calculated using Eq. (1), are shown below in figures 3-10. In addition to the percent errors, red lines are plotted to represent one standard deviation above from the percent errors. Areas where there are no red lines indicate values where the MCNP uncertainty was calculated by be 0.0000, or below the threshold of the MCNP output. There are also a few areas with percent uncertainties of 10^{-5} which indicate areas where the percent error is actually 0. These values were changed because there would otherwise be a break in the plots since it is a logarithmic plot.

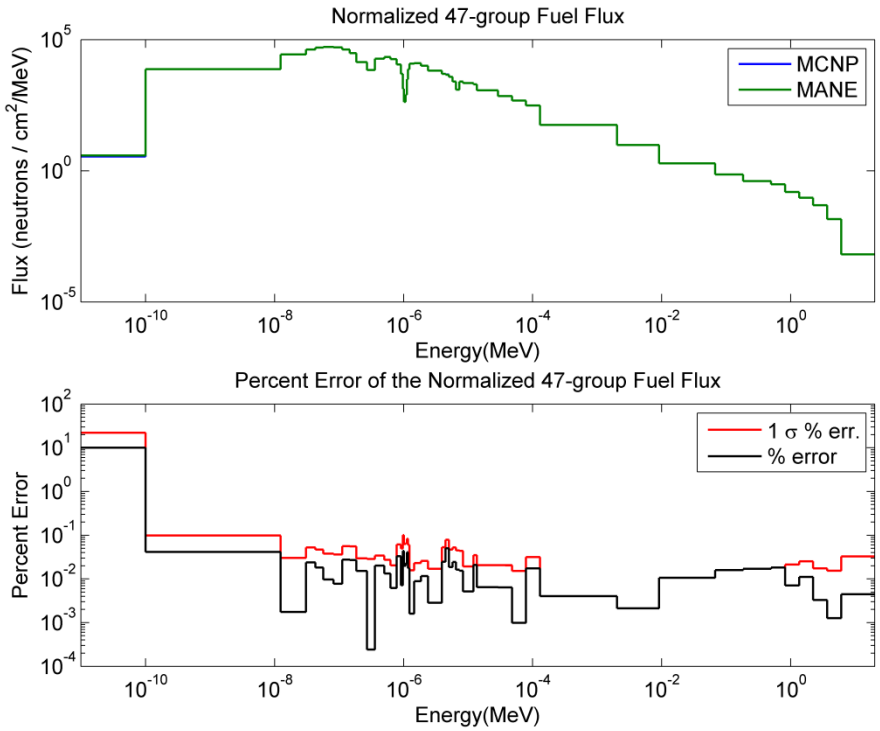

Figure 3: 47-group fuel flux for the MCNP and MANE run, and percent error.

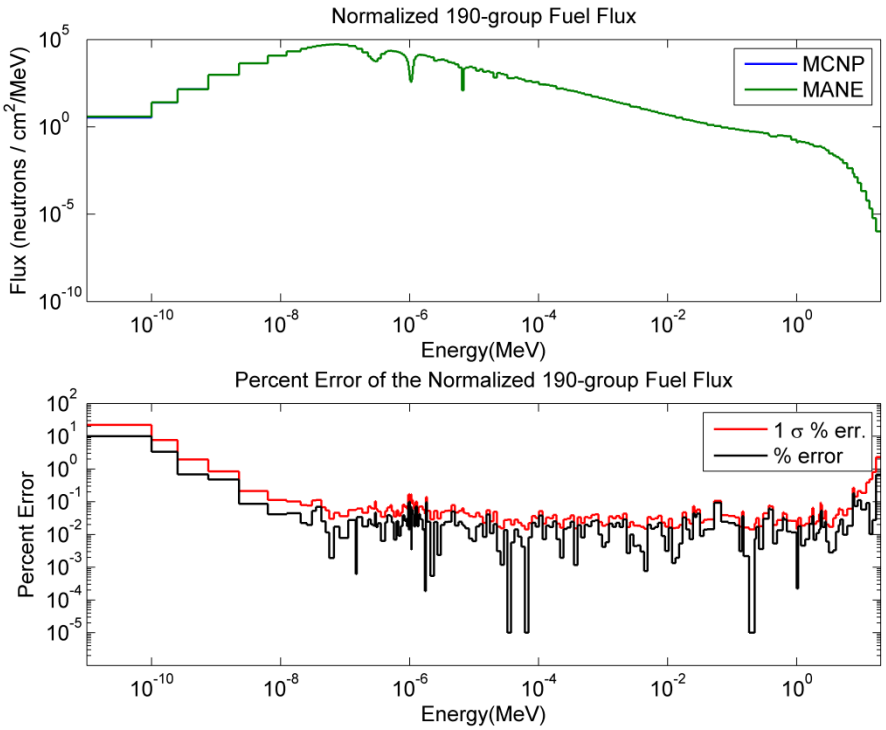

Figure 4: 190-group fuel flux for the MCNP and MANE run, and percent error.

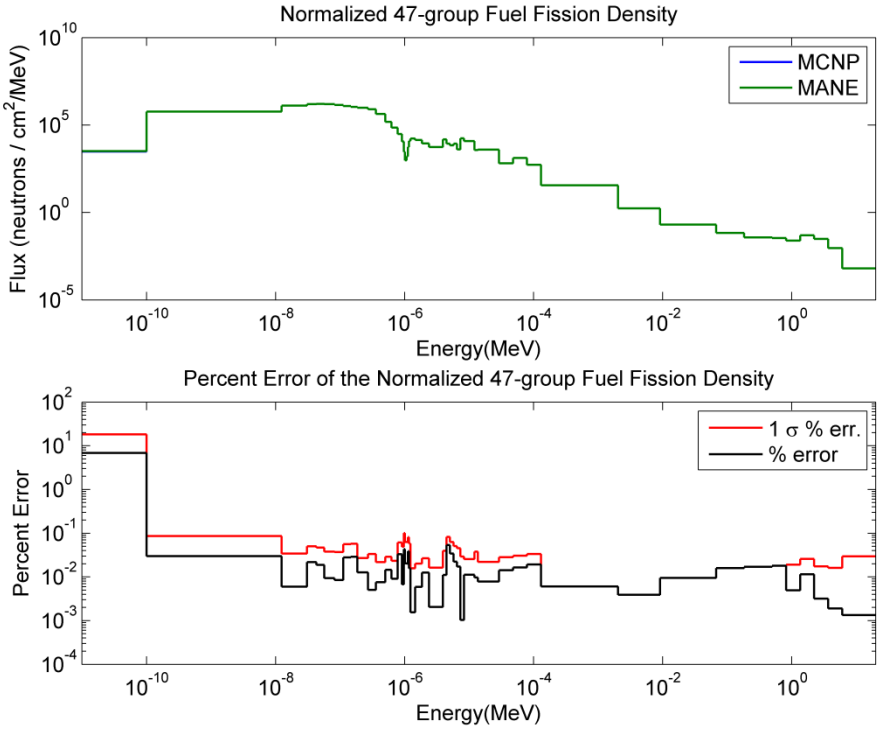

Figure 5: 47-group fuel fission density for the MCNP and MANE run, and percent error.

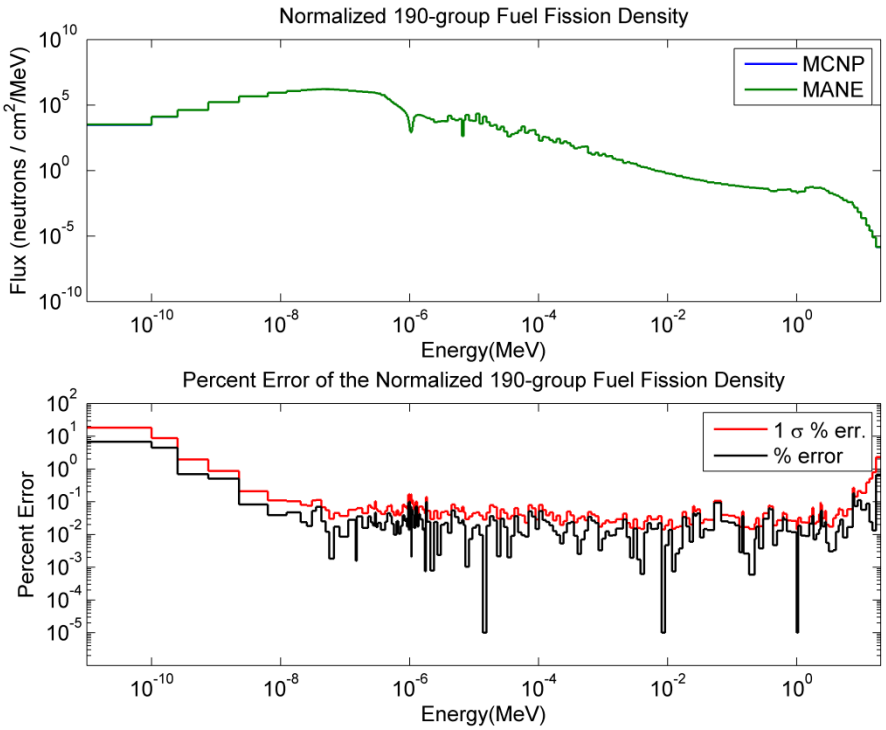

Figure 6: 190-group fuel fission density for the MCNP and MANE run, and percent error.

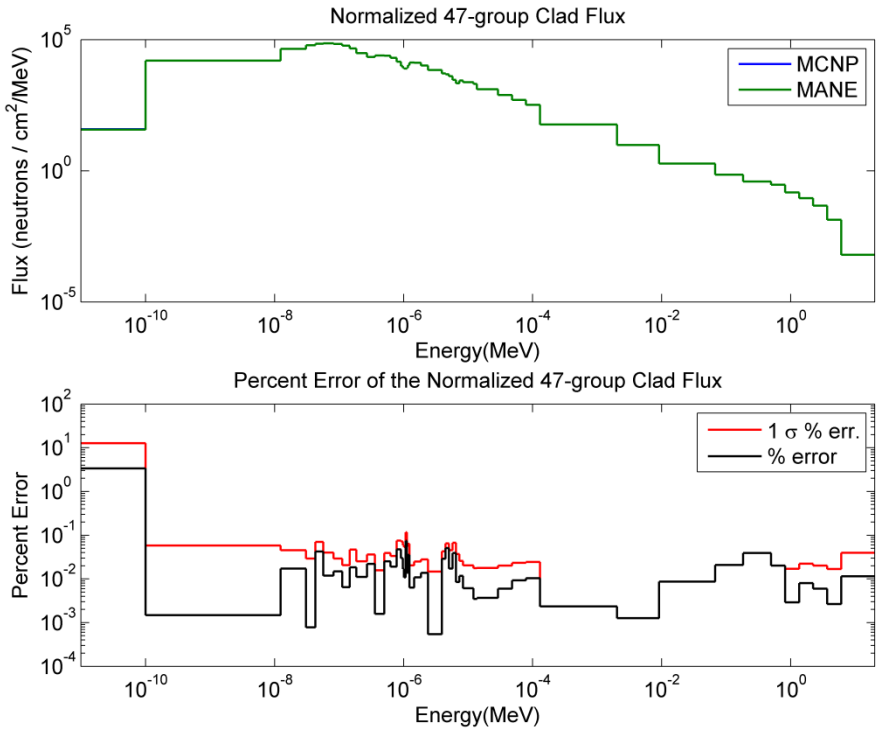

Figure 7: 47-group clad flux for the MCNP and MANE run, and percent error.

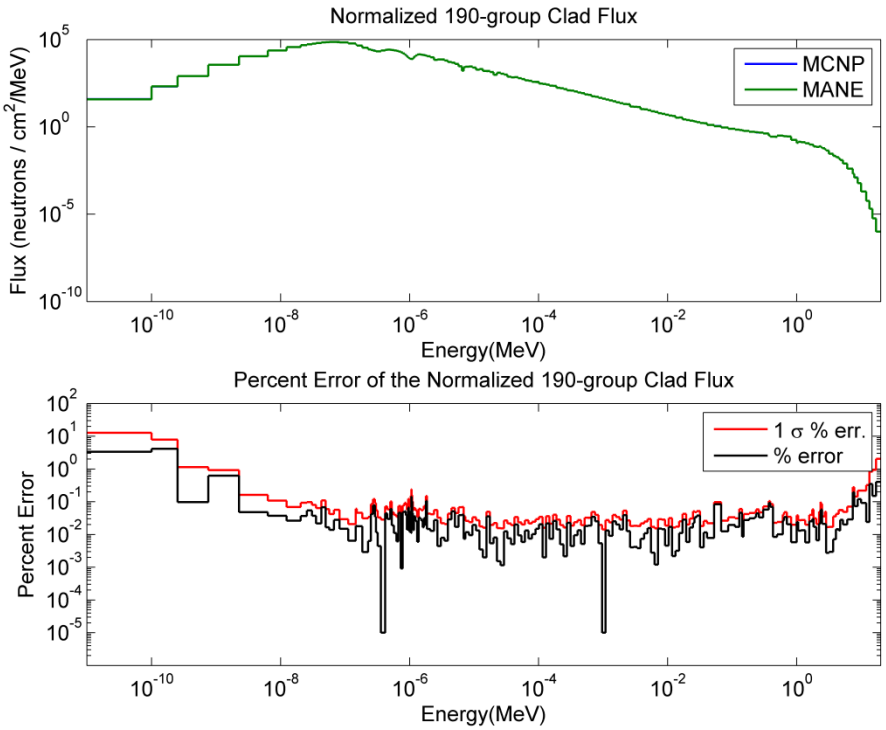

Figure 8: 190-group clad flux for the MCNP and MANE run, and percent error.

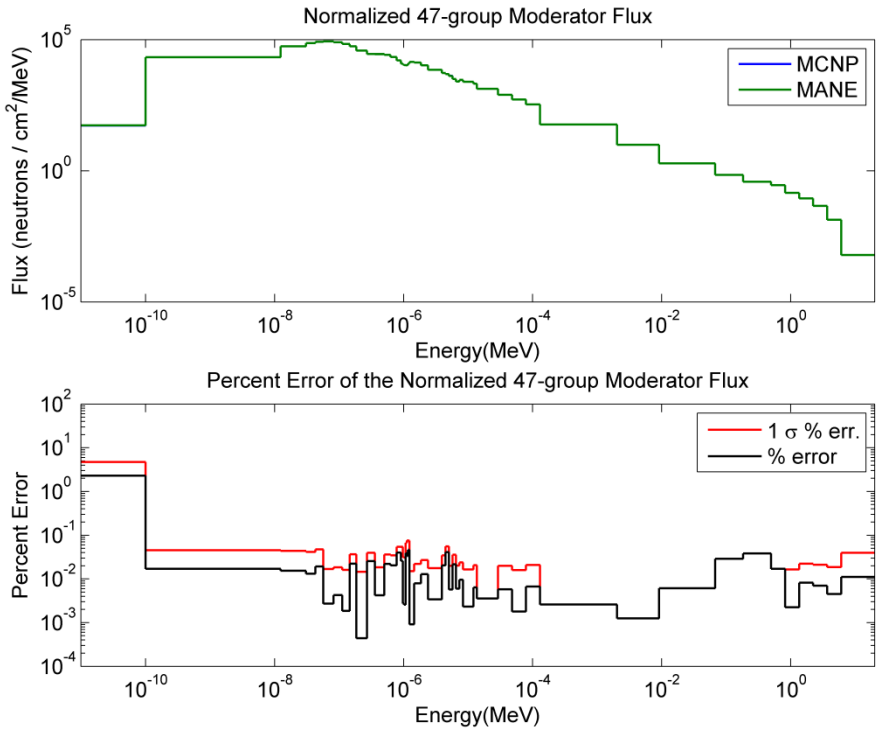

Figure 9: 47-group moderator flux for the MCNP and MANE run, and percent error.

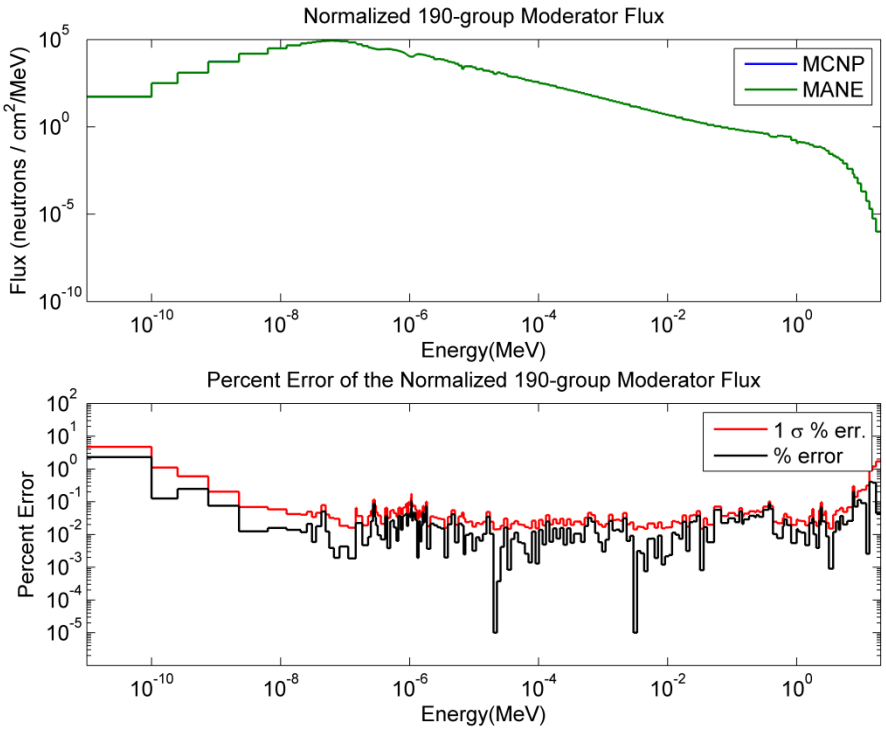

Figure 10: 190-group moderator flux for the MCNP and MANE run, and percent error.

Assembly

For each of the assemblies described below, the tallies were normalized using equation (6) below

$$F_i = \frac{f_i}{\sum_i f_i} \tag{6}$$

where f_i is the unnormalized tally in pin cell i. The same statistical metrics used to analyze the pin cell results were used to analyze the assembly-level results. Each assembly tallied up the fission density in the fuel rods, capture density in the fuel rods, and the 8-group flux in the moderator. The controlled UO_2 case also tallied the absorption density in the control rods.

Controlled UO_2

The results of the assembly eigenvalue are shown below in Table 5. As with the pin cell case, the small difference is due to the stochastic nature of MCNP and not because of any differences in the cross section sets.

Table 5: Controlled UO_2-level eigenvalue results

Cross Section Set	MCNP	MANE
K_∞	0.66805	0.66805
Standard Deviation (pcm)	2	2
Difference (pcm)	-	0

A table of total tally statistics is shown below in Table 6, and the energy-dependent moderator flux statistics are shown in Table 7. The relative uncertainties (UNC) in the tallies from MCNP are also shown for comparison in each of the tables.

Table 6: Controlled UO_2 assembly total tally results

Tally	MAX & S.D. (%)	AVG (%)	RMS (%)	MRE (%)	UNC (%)
Fission Density	0.150 (0.043)	0.040	0.049	0.040	0.031
Capture Density	0.152 (0.042)	0.038	0.047	0.035	0.030
Absorption Density	0.054 (0.029)	0.022	0.027	0.021	0.020
Moderator Flux	0.043 (0.014)	0.012	0.015	0.012	0.010

Table 7: Controlled UO_2 assembly energy dependent moderator flux results

Energy (MeV)	MAX & S.D. (%)	AVG (%)	RMS (%)	MRE (%)	UNC (%)
1.46E-07	0.199 (0.071)	0.056	0.069	0.056	0.051
6.25E-07	0.260 (0.071)	0.057	0.070	0.057	0.047
3.93E-06	0.192 (0.057)	0.052	0.065	0.052	0.042
1.30E-04	0.123 (0.042)	0.035	0.043	0.035	0.030
9.12E-03	0.113 (0.028)	0.025	0.032	0.025	0.020
8.21E-01	0.066 (0.028)	0.019	0.023	0.019	0.020
2.23E+00	0.126 (0.042)	0.029	0.036	0.029	0.022
2.00E+01	0.113 (0.042)	0.030	0.037	0.030	0.030

In each of the above tables, the AVG is in good agreement with the uncertainty. Just as with the pin cell case, the moderator flux value is in better agreement than the tallies in the fuel and control rod because of the similarities between the cross sections. The differences in the unresolved resonance tables for the fuel and control rod materials do not have a significant effect on these tallies or the criticality, which is within the statistical uncertainties calculated by MCNP.

In addition, maps of the percent errors as well as the standard deviation in the percent errors for each of the tallies are shown in Figure 11-14. In these figures, the number in the white cell is the percent error of the tally, and the number in the gray cell is the standard deviation of the percent error obtained by equation (7) below

$$\sigma_p = \sqrt{\frac{R_{mane}^2 X_{mane}^2}{X_{mcnp}^2} + \frac{R_{mcnp}^2 X_{mane}^2}{X_{mcnp}^2}} \tag{7}$$

where R_i is the relative error given in the MCNP output file from the MANE or MCNP run, and X_i is the tally given in the MCNP output file from the MANE or MCNP run. The plots are color coded to show how many standard deviations away each pin is. White is within 1 standard deviation, green is between 1-2 standard deviations, yellow is between 2-3 standard deviations, red is between 3-4 standard deviations, and dark red is between 4-5 standard deviations. Beneath each of the figures are tables (Tables 8-11) that describe what percent of each tally are less than each standard deviation compared against what the Gaussian distribution standard deviations are.

0.04	0.02	0.06	0.04	0.08	0.05	0.00	0.04	0.02	0.03	0.00	0.02	0.04	0.07	0.06	0.11	0.02
0.06	0.04	0.04	0.04	0.04	0.06	0.06	0.06	0.06	0.06	0.06	0.06	0.04	0.04	0.04	0.04	0.06
0.05	0.02	0.05	0.03	0.04	0.05	0.00	0.02	0.02	0.03	0.01	0.02	0.04	0.08	0.01	0.03	0.02
0.04	0.04	0.04	0.04	0.04	0.04	0.04	0.04	0.04	0.04	0.04	0.04	0.04	0.04	0.04	0.04	0.04
0.02	0.01	0.05	0.07	0.13		0.05	0.06		0.07	0.08		0.03	0.02	0.04	0.01	0.03
0.04	0.04	0.04	0.04	0.04		0.04	0.04		0.04	0.04		0.04	0.04	0.04	0.04	0.04
0.00	0.05	0.01		0.09	0.01	0.02	0.09	0.06	0.03	0.05	0.08	0.04		0.05	0.01	0.07
0.04	0.04	0.04		0.04	0.04	0.04	0.04	0.04	0.04	0.04	0.04	0.04		0.04	0.04	0.04
0.02	0.06	0.04	0.01	0.04	0.09	0.03	0.01	0.03	0.01	0.04	0.02	0.01	0.01	0.04	0.04	0.10
0.04	0.04	0.04	0.04	0.04	0.04	0.04	0.04	0.04	0.04	0.04	0.04	0.04	0.04	0.04	0.04	0.04
0.09	0.02		0.11	0.03		0.09	0.05		0.01	0.02		0.02	0.03		0.07	0.06
0.06	0.04		0.04	0.04		0.04	0.04		0.04	0.04		0.04	0.04		0.04	0.06
0.06	0.02	0.01	0.07	0.01	0.05	0.02	0.08	0.06	0.05	0.01	0.04	0.04	0.00	0.05	0.03	0.01
0.06	0.04	0.04	0.04	0.04	0.04	0.04	0.04	0.04	0.04	0.04	0.04	0.04	0.04	0.04	0.04	0.06
0.05	0.01	0.06	0.06	0.01	0.02	0.05	0.00	0.03	0.06	0.02	0.03	0.02	0.02	0.02	0.05	0.02
0.06	0.04	0.04	0.04	0.04	0.04	0.04	0.04	0.04	0.04	0.04	0.04	0.04	0.04	0.04	0.04	0.06
0.04	0.08		0.04	0.02		0.09	0.00		0.03	0.04		0.08	0.03		0.01	0.01
0.06	0.04		0.04	0.04		0.04	0.04		0.04	0.04		0.04	0.04		0.04	0.06
0.03	0.06	0.01	0.03	0.02	0.01	0.04	0.01	0.11	0.05	0.01	0.02	0.02	0.03	0.05	0.06	0.07
0.06	0.04	0.04	0.04	0.04	0.04	0.04	0.04	0.04	0.04	0.04	0.04	0.04	0.04	0.04	0.04	0.06
0.01	0.05	0.05	0.13	0.03	0.04	0.01	0.05	0.01	0.04	0.07	0.01	0.02	0.06	0.09	0.03	0.10
0.06	0.04	0.04	0.04	0.04	0.04	0.04	0.04	0.04	0.04	0.04	0.04	0.04	0.04	0.04	0.04	0.06
0.05	0.02		0.10	0.02		0.07	0.06		0.01	0.01		0.01	0.04		0.00	0.02
0.05	0.04		0.04	0.04		0.04	0.04		0.04	0.04		0.04	0.04		0.04	0.06
0.06	0.00	0.05	0.06	0.00	0.01	0.10	0.08	0.01	0.04	0.03	0.00	0.07	0.09	0.03	0.05	0.00
0.04	0.04	0.04	0.04	0.04	0.04	0.04	0.04	0.04	0.04	0.04	0.04	0.04	0.04	0.04	0.04	0.04
0.04	0.02	0.15		0.04	0.02	0.01	0.00	0.08	0.03	0.03	0.01	0.05		0.05	0.02	0.02
0.04	0.04	0.04		0.04	0.04	0.04	0.04	0.04	0.04	0.04	0.04	0.04		0.04	0.04	0.04
0.07	0.03	0.01	0.01	0.02		0.00	0.08		0.04	0.09		0.01	0.14	0.04	0.02	0.00
0.04	0.04	0.04	0.04	0.04		0.04	0.04		0.04	0.04		0.04	0.04	0.04	0.04	0.04
0.02	0.05	0.01	0.01	0.02	0.06	0.01	0.03	0.03	0.08	0.06	0.05	0.02	0.08	0.05	0.03	0.06
0.04	0.04	0.04	0.04	0.04	0.04	0.04	0.04	0.04	0.04	0.04	0.04	0.04	0.04	0.04	0.04	0.04
0.02	0.02	0.06	0.03	0.03	0.00	0.06	0.08	0.06	0.01	0.06	0.05	0.11	0.06	0.10	0.02	0.02
0.06	0.04	0.04	0.04	0.04	0.06	0.06	0.06	0.06	0.06	0.06	0.06	0.04	0.04	0.04	0.04	0.06

Figure 11: Controlled UO_2 assembly percent error of the fission density in the fuel rods and standard deviation of the percent error

Table 8: Distribution of controlled UO_2 assembly tally results of the fission density in the fuel rods compared against a Gaussian distribution

	Fission Density (%)	Gaussian Distribution (%)
1 σ	59.8484848	68.2689492
2 σ	92.8030303	95.4499736
3 σ	98.4848485	99.7300203
4 σ	100.0000000	99.9936657
5 σ	100.0000000	99.9999426

0.03	0.08	0.06	0.07	0.06	0.06	0.00	0.02	0.05	0.04	0.03	0.01	0.02	0.06	0.07	0.06	0.03
0.04	0.04	0.04	0.04	0.04	0.04	0.04	0.04	0.04	0.04	0.04	0.04	0.04	0.04	0.04	0.04	0.04
0.00	0.05	0.02	0.02	0.04	0.05	0.00	0.01	0.01	0.02	0.03	0.02	0.00	0.07	0.05	0.01	0.02
0.04	0.04	0.04	0.04	0.04	0.04	0.04	0.04	0.04	0.04	0.04	0.04	0.04	0.04	0.04	0.04	0.04
0.04	0.06	0.02	0.08	0.06		0.02	0.01		0.02	0.05		0.06	0.00	0.05	0.00	0.01
0.04	0.04	0.04	0.04	0.04		0.04	0.04		0.04	0.04		0.04	0.04	0.04	0.04	0.04
0.04	0.02	0.01		0.06	0.01	0.07	0.09	0.03	0.07	0.05	0.10	0.03		0.00	0.01	0.04
0.04	0.04	0.04		0.04	0.04	0.04	0.04	0.04	0.04	0.04	0.04	0.04		0.04	0.04	0.04
0.00	0.05	0.03	0.03	0.03	0.04	0.06	0.01	0.06	0.02	0.04	0.00	0.01	0.03	0.01	0.03	0.01
0.04	0.04	0.04	0.04	0.04	0.04	0.04	0.04	0.04	0.04	0.04	0.04	0.04	0.04	0.04	0.04	0.04
0.03	0.01		0.03	0.03		0.05	0.03		0.02	0.09		0.03	0.06		0.02	0.09
0.04	0.04		0.04	0.04		0.04	0.04		0.04	0.04		0.04	0.04		0.04	0.04
0.03	0.02	0.02	0.10	0.02	0.02	0.02	0.15	0.05	0.02	0.09	0.02	0.04	0.03	0.03	0.00	0.01
0.04	0.04	0.04	0.04	0.04	0.04	0.04	0.04	0.04	0.04	0.04	0.04	0.04	0.04	0.04	0.04	0.04
0.04	0.02	0.07	0.05	0.03	0.03	0.05	0.05	0.05	0.00	0.02	0.03	0.01	0.02	0.02	0.05	0.01
0.04	0.04	0.04	0.04	0.04	0.04	0.04	0.04	0.04	0.04	0.04	0.04	0.04	0.04	0.04	0.04	0.04
0.04	0.05		0.01	0.04		0.09	0.00		0.03	0.05		0.12	0.02		0.08	0.06
0.04	0.04		0.04	0.04		0.04	0.04		0.04	0.04		0.04	0.04		0.04	0.04
0.02	0.01	0.05	0.00	0.00	0.01	0.02	0.06	0.09	0.01	0.03	0.01	0.03	0.00	0.02	0.06	0.04
0.04	0.04	0.04	0.04	0.04	0.04	0.04	0.04	0.04	0.04	0.04	0.04	0.04	0.04	0.04	0.04	0.04
0.02	0.03	0.03	0.11	0.05	0.08	0.04	0.00	0.06	0.01	0.05	0.06	0.05	0.07	0.06	0.07	0.07
0.04	0.04	0.04	0.04	0.04	0.04	0.04	0.04	0.04	0.04	0.04	0.04	0.04	0.04	0.04	0.04	0.04
0.05	0.00		0.06	0.05		0.03	0.05		0.01	0.03		0.02	0.02		0.00	0.05
0.04	0.04		0.04	0.04		0.04	0.04		0.04	0.04		0.04	0.04		0.04	0.04
0.07	0.04	0.04	0.04	0.02	0.03	0.11	0.07	0.04	0.03	0.04	0.01	0.10	0.04	0.06	0.08	0.04
0.04	0.04	0.04	0.04	0.04	0.04	0.04	0.04	0.04	0.04	0.04	0.04	0.04	0.04	0.04	0.04	0.04
0.07	0.03	0.10		0.03	0.03	0.02	0.00	0.05	0.03	0.03	0.04	0.01		0.06	0.01	0.02
0.04	0.04	0.04		0.04	0.04	0.04	0.04	0.04	0.04	0.04	0.04	0.04		0.04	0.04	0.04
0.08	0.05	0.02	0.03	0.01		0.04	0.05		0.05	0.00		0.03	0.11	0.05	0.07	0.05
0.04	0.04	0.04	0.04	0.04		0.04	0.04		0.04	0.04		0.04	0.04	0.04	0.04	0.04
0.02	0.08	0.01	0.02	0.01	0.03	0.04	0.01	0.02	0.07	0.08	0.03	0.04	0.10	0.08	0.02	0.03
0.04	0.04	0.04	0.04	0.04	0.04	0.04	0.04	0.04	0.04	0.04	0.04	0.04	0.04	0.04	0.04	0.04
0.01	0.05	0.01	0.01	0.01	0.05	0.01	0.02	0.09	0.00	0.03	0.03	0.04	0.10	0.08	0.04	0.01
0.04	0.04	0.04	0.04	0.04	0.04	0.04	0.04	0.04	0.04	0.04	0.04	0.04	0.04	0.04	0.04	0.04

Figure 12: Controlled UO_2 assembly percent error of the capture density in the fuel rods and standard deviation of the percent error

Table 9: Distribution of controlled UO_2 assembly tally results of the capture density in the fuel rods compared against a Gaussian distribution

	Capture Density (%)	Gaussian Distribution (%)
1 σ	62.5000000	68.2689492
2 σ	93.1818182	95.4499736
3 σ	99.6212121	99.7300203
4 σ	100.0000000	99.9936657
5 σ	100.0000000	99.9999426

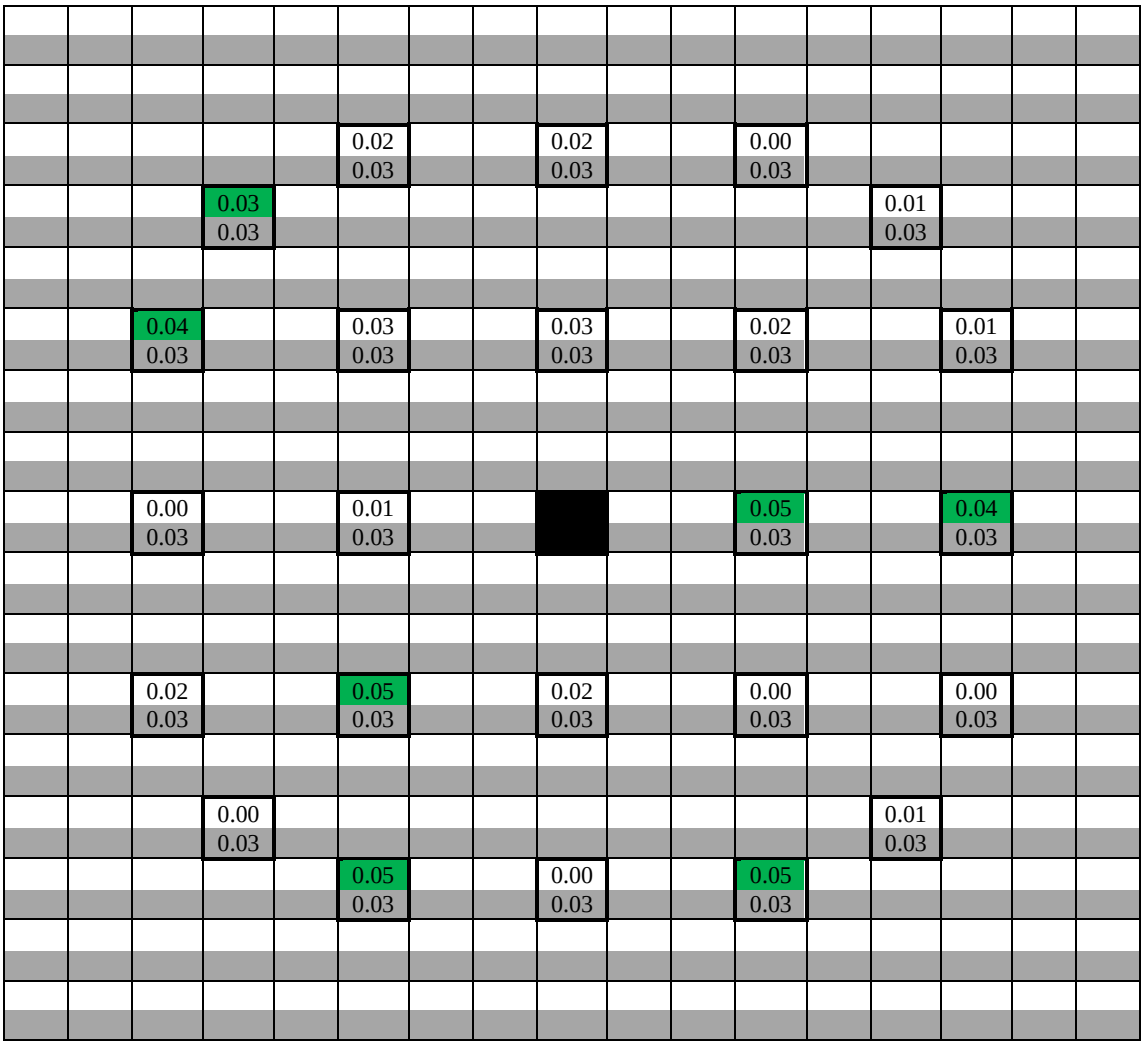

Figure 13: Controlled UO_2 assembly percent error of the absorption density in the control rods and standard deviation of the percent error

Table 10: Distribution of controlled UO_2 assembly tally results of the absorption density in the control rods compared against a Gaussian distribution

	Absorption Density (%)	Gaussian Distribution (%)
1 σ	70.8333333	68.2689492
2 σ	100.0000000	95.4499736
3 σ	100.0000000	99.7300203
4 σ	100.0000000	99.9936657
5 σ	100.0000000	99.9999426

0.01	0.03	0.02	0.00	0.00	0.02	0.00	0.01	0.01	0.01	0.01	0.01	0.01	0.01	0.03	0.01	0.01
0.01	0.01	0.01	0.01	0.01	0.01	0.01	0.01	0.01	0.01	0.01	0.01	0.01	0.01	0.01	0.01	0.01
0.00	0.04	0.04	0.00	0.01	0.02	0.01	0.02	0.00	0.00	0.00	0.01	0.01	0.02	0.01	0.00	0.01
0.01	0.01	0.01	0.01	0.01	0.01	0.01	0.01	0.01	0.01	0.01	0.01	0.01	0.01	0.01	0.01	0.01
0.03	0.01	0.00	0.00	0.00	0.01	0.01	0.00	0.01	0.01	0.01	0.01	0.01	0.01	0.03	0.02	0.01
0.01	0.01	0.01	0.01	0.01	0.01	0.01	0.01	0.01	0.01	0.01	0.01	0.01	0.01	0.01	0.01	0.01
0.00	0.01	0.00	0.00	0.01	0.01	0.00	0.00	0.03	0.02	0.02	0.01	0.01	0.02	0.00	0.01	0.01
0.01	0.01	0.01	0.01	0.01	0.01	0.01	0.01	0.01	0.01	0.01	0.01	0.01	0.01	0.01	0.01	0.01
0.01	0.03	0.01	0.01	0.00	0.01	0.01	0.02	0.02	0.02	0.02	0.01	0.03	0.01	0.00	0.02	0.02
0.01	0.01	0.01	0.01	0.01	0.01	0.01	0.01	0.01	0.01	0.01	0.01	0.01	0.01	0.01	0.01	0.01
0.02	0.02	0.00	0.02	0.01	0.02	0.03	0.02	0.03	0.02	0.03	0.02	0.01	0.01	0.00	0.00	0.00
0.01	0.01	0.01	0.01	0.01	0.01	0.01	0.01	0.01	0.01	0.01	0.01	0.01	0.01	0.01	0.01	0.01
0.03	0.03	0.01	0.00	0.01	0.01	0.02	0.01	0.00	0.01	0.01	0.00	0.01	0.00	0.02	0.01	0.00
0.01	0.01	0.01	0.01	0.01	0.01	0.01	0.01	0.01	0.01	0.01	0.01	0.01	0.01	0.01	0.01	0.01
0.01	0.01	0.00	0.00	0.00	0.01	0.00	0.00	0.00	0.01	0.01	0.00	0.01	0.01	0.00	0.01	0.01
0.01	0.01	0.01	0.01	0.01	0.01	0.01	0.01	0.01	0.01	0.01	0.01	0.01	0.01	0.01	0.01	0.01
0.00	0.00	0.00	0.00	0.02	0.02	0.02	0.01	0.02	0.01	0.01	0.00	0.01	0.00	0.01	0.00	0.01
0.01	0.01	0.01	0.01	0.01	0.01	0.01	0.01	0.01	0.01	0.01	0.01	0.01	0.01	0.01	0.01	0.01
0.01	0.01	0.02	0.02	0.03	0.01	0.01	0.01	0.02	0.01	0.01	0.00	0.01	0.00	0.02	0.02	0.03
0.01	0.01	0.01	0.01	0.01	0.01	0.01	0.01	0.01	0.01	0.01	0.01	0.01	0.01	0.01	0.01	0.01
0.00	0.02	0.00	0.03	0.00	0.02	0.01	0.03	0.01	0.00	0.00	0.01	0.01	0.00	0.01	0.03	0.02
0.01	0.01	0.01	0.01	0.01	0.01	0.01	0.01	0.01	0.01	0.01	0.01	0.01	0.01	0.01	0.01	0.01
0.02	0.04	0.02	0.01	0.00	0.02	0.00	0.03	0.02	0.01	0.01	0.01	0.02	0.00	0.02	0.01	0.00
0.01	0.01	0.01	0.01	0.01	0.01	0.01	0.01	0.01	0.01	0.01	0.01	0.01	0.01	0.01	0.01	0.01
0.02	0.04	0.02	0.01	0.01	0.02	0.02	0.00	0.01	0.01	0.02	0.01	0.01	0.01	0.01	0.01	0.00
0.01	0.01	0.01	0.01	0.01	0.01	0.01	0.01	0.01	0.01	0.01	0.01	0.01	0.01	0.01	0.01	0.01
0.00	0.01	0.00	0.00	0.01	0.00	0.02	0.01	0.00	0.01	0.00	0.01	0.01	0.01	0.01	0.01	0.00
0.01	0.01	0.01	0.01	0.01	0.01	0.01	0.01	0.01	0.01	0.01	0.01	0.01	0.01	0.01	0.01	0.01
0.00	0.00	0.01	0.02	0.01	0.02	0.02	0.00	0.01	0.01	0.00	0.02	0.02	0.01	0.01	0.00	0.02
0.01	0.01	0.01	0.01	0.01	0.01	0.01	0.01	0.01	0.01	0.01	0.01	0.01	0.01	0.01	0.01	0.01
0.01	0.01	0.03	0.02	0.01	0.01	0.00	0.01	0.01	0.02	0.03	0.02	0.02	0.03	0.02	0.01	0.00
0.01	0.01	0.01	0.01	0.01	0.01	0.01	0.01	0.01	0.01	0.01	0.01	0.01	0.01	0.01	0.01	0.01
0.00	0.01	0.02	0.02	0.01	0.01	0.01	0.01	0.02	0.02	0.01	0.03	0.03	0.02	0.01	0.04	0.01
0.01	0.01	0.01	0.01	0.01	0.01	0.01	0.01	0.01	0.01	0.01	0.01	0.01	0.01	0.01	0.01	0.01

Figure 14: Controlled UO_2 assembly percent error of the moderator flux and standard deviation of the percent error

Table 11: Distribution of controlled UO_2 assembly tally results of the moderator flux compared against a Gaussian distribution

	Moderator Flux (%)	Gaussian Distribution (%)
1 σ	65.7439446	68.2689492
2 σ	94.1176471	95.4499736
3 σ	99.6539792	99.7300203
4 σ	100.0000000	99.9936657
5 σ	100.0000000	99.9999426

From figures 11-14 on the previous pages, the location of the percent errors appears sporadic and does not have any noticeable effects from boundary conditions or proximity near control rod materials. In the capture and fission densities, the largest percent errors occur in the same pins, but the order of those errors from largest to smallest is not necessarily the same between the two tallies (e.g. the largest fission density error is not in the same cell as the largest capture density error). This is due to other cross sections represented by the unresolved probability tables, which are used in the capture tally (the capture cross section) and were not used in the fission density tally. This would lead to different cells having different maximum errors. The uncertainties in the moderator flux are much smaller than the uncertainties in the tally densities. One unique feature of the absorption density statistics is that it does not seem to follow a Gaussian distribution. This can be attributed to the fact that there are only 24 control rods, as compared to 265 fuel rods. This smaller sample size makes the aberration from the Gaussian distribution acceptable. This comes from the density tallies having uncertainties propagated from the cross sections. Since the moderator flux is not directly multiplied by a cross section to produce a density tally like the other tallies, and subsequently no cross section uncertainties to propagate, the uncertainties here would be smaller.

Uncontrolled UO_2

The results of the assembly eigenvalue are shown below in Table 12 As with the controlled UO_2 case, the agreement between the two runs is very good.

Table 12: Uncontrolled UO_2 assembly eigenvalue results

Cross Section Set	MCNP	MANE
K_∞	1.07882	1.07883
Standard Deviation (pcm)	2	2
Difference (pcm)	-	1

A table of total tally statistics is shown below in Table 13, and the energy-dependent moderator flux statistics are shown in Table 14. In addition, maps of the percent errors as well as the error in the percent errors for each of the tallies are shown in Figure 15-17. The coloring scheme from the controlled UO_2 case is employed in these figures as well. Tables 15-17, shown beneath these figures 15-17, shows the same statistical representations as in the controlled UO_2 case.

Table 13: Uncontrolled UO_2 assembly total tally results

Tally	MAX & S.D. (%)	AVG (%)	RMS (%)	MRE (%)	UNC (%)
Fission Density	0.132 (0.043)	0.033	0.041	0.033	0.030
Capture Density	0.121 (0.042)	0.030	0.039	0.030	0.030
Moderator Flux	0.066 (0.014)	0.013	0.017	0.013	0.010

Table 14: Uncontrolled UO_2 assembly energy dependent moderator flux results

Energy (MeV)	MAX & S.D. (%)	AVG (%)	RMS (%)	MRE (%)	UNC (%)
1.46E-07	0.159 (0.042)	0.042	0.054	0.042	0.034
6.25E-07	0.136 (0.056)	0.040	0.049	0.040	0.033
3.93E-06	0.161 (0.056)	0.042	0.053	0.042	0.035
1.30E-04	0.125 (0.042)	0.030	0.038	0.030	0.030
9.12E-03	0.124 (0.042)	0.028	0.037	0.028	0.022
8.21E-01	0.080 (0.028)	0.021	0.026	0.021	0.020
2.23E+00	0.098 (0.028)	0.027	0.034	0.027	0.023
2.00E+01	0.109 (0.042)	0.031	0.038	0.031	0.030

The errors for the uncontrolled UO_2 assembly are, on average, in better agreement than the results from the controlled UO_2 assembly. Because there are no control rods in the uncontrolled case, the flux would be flatter throughout the assembly, which means it is less likely there would be any disagreement due to large gradients in the flux caused by control rods. As with the controlled UO_2 case, all of the average percent errors are near the statistical uncertainties calculated by MCNP.

0.01	0.02	0.00	0.07	0.03	0.06	0.01	0.10	0.00	0.06	0.02	0.02	0.00	0.00	0.04	0.05	0.04
0.06	0.04	0.04	0.04	0.04	0.04	0.04	0.04	0.04	0.04	0.04	0.04	0.04	0.04	0.04	0.04	0.06
0.01	0.05	0.05	0.01	0.05	0.05	0.01	0.01	0.00	0.02	0.01	0.11	0.03	0.04	0.02	0.06	0.01
0.04	0.04	0.04	0.04	0.04	0.04	0.04	0.04	0.04	0.04	0.04	0.04	0.04	0.04	0.04	0.04	0.04
0.01	0.01	0.05	0.01	0.00		0.07	0.03		0.07	0.02		0.02	0.03	0.06	0.02	0.01
0.04	0.04	0.04	0.04	0.04		0.04	0.04		0.04	0.04		0.04	0.04	0.04	0.04	0.04
0.02	0.04	0.01		0.03	0.02	0.04	0.07	0.03	0.03	0.06	0.03	0.04		0.01	0.03	0.03
0.04	0.04	0.04		0.04	0.04	0.04	0.04	0.04	0.04	0.04	0.04	0.04		0.04	0.04	0.04
0.01	0.03	0.00	0.01	0.02	0.02	0.00	0.05	0.00	0.05	0.00	0.01	0.13	0.03	0.06	0.03	0.09
0.04	0.04	0.04	0.04	0.04	0.04	0.04	0.04	0.04	0.04	0.04	0.04	0.04	0.04	0.04	0.04	0.04
0.05	0.02		0.01	0.01		0.01	0.03		0.06	0.00		0.11	0.01		0.03	0.07
0.04	0.04		0.04	0.04		0.04	0.04		0.04	0.04		0.04	0.04		0.04	0.04
0.06	0.08	0.10	0.04	0.03	0.05	0.09	0.06	0.02	0.01	0.04	0.02	0.00	0.04	0.06	0.06	0.01
0.04	0.04	0.04	0.04	0.04	0.04	0.04	0.04	0.04	0.04	0.04	0.04	0.04	0.04	0.04	0.04	0.04
0.03	0.04	0.03	0.04	0.02	0.05	0.01	0.02	0.04	0.04	0.01	0.00	0.00	0.01	0.09	0.07	0.09
0.04	0.04	0.04	0.04	0.04	0.04	0.04	0.04	0.04	0.04	0.04	0.04	0.04	0.04	0.04	0.04	0.04
0.07	0.02		0.01	0.00		0.02	0.06		0.04	0.02		0.05	0.03		0.08	0.07
0.04	0.04		0.04	0.04		0.04	0.04		0.04	0.04		0.04	0.04		0.04	0.04
0.01	0.06	0.05	0.03	0.03	0.02	0.03	0.05	0.03	0.03	0.01	0.06	0.00	0.03	0.01	0.06	0.05
0.04	0.04	0.04	0.04	0.04	0.04	0.04	0.04	0.04	0.04	0.04	0.04	0.04	0.04	0.04	0.04	0.04
0.03	0.03	0.01	0.06	0.05	0.07	0.00	0.01	0.03	0.06	0.03	0.04	0.02	0.02	0.01	0.02	0.03
0.04	0.04	0.04	0.04	0.04	0.04	0.04	0.04	0.04	0.04	0.04	0.04	0.04	0.04	0.04	0.04	0.04
0.06	0.04		0.05	0.02		0.04	0.03		0.03	0.04		0.02	0.01		0.03	0.01
0.04	0.04		0.04	0.04		0.04	0.04		0.04	0.04		0.04	0.04		0.04	0.04
0.03	0.02	0.02	0.04	0.01	0.05	0.03	0.01	0.02	0.06	0.00	0.07	0.02	0.03	0.01	0.08	0.03
0.04	0.04	0.04	0.04	0.04	0.04	0.04	0.04	0.04	0.04	0.04	0.04	0.04	0.04	0.04	0.04	0.04
0.01	0.09	0.06		0.04	0.00	0.00	0.05	0.05	0.00	0.01	0.06	0.08		0.02	0.01	0.04
0.04	0.04	0.04		0.04	0.04	0.04	0.04	0.04	0.04	0.04	0.04	0.04		0.04	0.04	0.04
0.06	0.02	0.01	0.03	0.01		0.01	0.00		0.04	0.02		0.04	0.05	0.01	0.04	0.07
0.04	0.04	0.04	0.04	0.04		0.04	0.04		0.04	0.04		0.04	0.04	0.04	0.04	0.04
0.06	0.04	0.08	0.02	0.02	0.01	0.04	0.04	0.01	0.01	0.03	0.01	0.04	0.02	0.02	0.03	0.02
0.04	0.04	0.04	0.04	0.04	0.04	0.04	0.04	0.04	0.04	0.04	0.04	0.04	0.04	0.04	0.04	0.04
0.03	0.06	0.01	0.01	0.01	0.01	0.01	0.01	0.00	0.04	0.10	0.08	0.02	0.04	0.01	0.03	0.03
0.06	0.04	0.04	0.04	0.04	0.04	0.04	0.04	0.04	0.04	0.04	0.04	0.04	0.04	0.04	0.04	0.06

Figure 15: Uncontrolled UO_2 assembly percent error of the fission density in the fuel rods and standard deviation of the percent error

Table 15: Distribution of uncontrolled UO_2 assembly tally results of the fission density in the fuel rods compared against a Gaussian distribution

	Fission Density (%)	Gaussian Distribution (%)
1 σ	69.6969697	68.2689492
2 σ	95.8333333	95.4499736
3 σ	99.6212121	99.7300203
4 σ	100.0000000	99.9936657
5 σ	100.0000000	99.9999426

0.03	0.02	0.00	0.05	0.03	0.01	0.02	0.06	0.01	0.06	0.01	0.04	0.03	0.02	0.01	0.05	0.03
0.04	0.04	0.04	0.04	0.04	0.04	0.04	0.04	0.04	0.04	0.04	0.04	0.04	0.04	0.04	0.04	0.04
0.02	0.04	0.05	0.05	0.02	0.02	0.04	0.00	0.03	0.01	0.00	0.07	0.05	0.05	0.01	0.01	0.01
0.04	0.04	0.04	0.04	0.04	0.04	0.04	0.04	0.04	0.04	0.04	0.04	0.04	0.04	0.04	0.04	0.04
0.02	0.02	0.05	0.03	0.00		0.08	0.06		0.12	0.04		0.02	0.01	0.00	0.01	0.00
0.04	0.04	0.04	0.04	0.04		0.04	0.04		0.04	0.04		0.04	0.04	0.04	0.04	0.04
0.07	0.00	0.01		0.01	0.03	0.05	0.03	0.01	0.03	0.01	0.03	0.05		0.01	0.01	0.05
0.04	0.04	0.04		0.04	0.04	0.04	0.04	0.04	0.04	0.04	0.04	0.04		0.04	0.04	0.04
0.01	0.02	0.02	0.03	0.04	0.01	0.01	0.08	0.00	0.03	0.03	0.03	0.12	0.05	0.08	0.03	0.08
0.04	0.04	0.04	0.04	0.04	0.04	0.04	0.04	0.04	0.04	0.04	0.04	0.04	0.04	0.04	0.04	0.04
0.10	0.00		0.02	0.01		0.04	0.05		0.05	0.01		0.08	0.04		0.01	0.02
0.04	0.04		0.04	0.04		0.04	0.04		0.04	0.04		0.04	0.04		0.04	0.04
0.09	0.06	0.07	0.00	0.01	0.02	0.07	0.08	0.00	0.03	0.05	0.01	0.04	0.02	0.05	0.01	0.02
0.04	0.04	0.04	0.04	0.04	0.04	0.04	0.04	0.04	0.04	0.04	0.04	0.04	0.04	0.04	0.04	0.04
0.01	0.04	0.00	0.00	0.04	0.00	0.02	0.04	0.02	0.02	0.01	0.04	0.02	0.02	0.05	0.05	0.08
0.04	0.04	0.04	0.04	0.04	0.04	0.04	0.04	0.04	0.04	0.04	0.04	0.04	0.04	0.04	0.04	0.04
0.07	0.06		0.03	0.00		0.01	0.02		0.03	0.02		0.03	0.00		0.08	0.05
0.04	0.04		0.04	0.04		0.04	0.04		0.04	0.04		0.04	0.04		0.04	0.04
0.01	0.01	0.02	0.01	0.00	0.04	0.07	0.02	0.06	0.02	0.02	0.10	0.04	0.06	0.01	0.02	0.07
0.04	0.04	0.04	0.04	0.04	0.04	0.04	0.04	0.04	0.04	0.04	0.04	0.04	0.04	0.04	0.04	0.04
0.01	0.04	0.01	0.02	0.06	0.07	0.03	0.01	0.05	0.01	0.05	0.06	0.00	0.05	0.05	0.01	0.01
0.04	0.04	0.04	0.04	0.04	0.04	0.04	0.04	0.04	0.04	0.04	0.04	0.04	0.04	0.04	0.04	0.04
0.00	0.05		0.00	0.00		0.00	0.03		0.05	0.01		0.01	0.06		0.00	0.01
0.04	0.04		0.04	0.04		0.04	0.04		0.04	0.04		0.04	0.04		0.04	0.04
0.00	0.02	0.07	0.02	0.02	0.03	0.00	0.05	0.00	0.02	0.02	0.04	0.01	0.04	0.04	0.04	0.02
0.04	0.04	0.04	0.04	0.04	0.04	0.04	0.04	0.04	0.04	0.04	0.04	0.04	0.04	0.04	0.04	0.04
0.03	0.05	0.06		0.03	0.01	0.01	0.03	0.02	0.01	0.02	0.05	0.11		0.06	0.01	0.05
0.04	0.04	0.04		0.04	0.04	0.04	0.04	0.04	0.04	0.04	0.04	0.04		0.04	0.04	0.04
0.03	0.02	0.00	0.00	0.02		0.00	0.02		0.03	0.04		0.02	0.07	0.01	0.07	0.02
0.04	0.04	0.04	0.04	0.04		0.04	0.04		0.04	0.04		0.04	0.04	0.04	0.04	0.04
0.05	0.02	0.08	0.03	0.01	0.03	0.02	0.00	0.01	0.01	0.04	0.04	0.03	0.00	0.00	0.05	0.02
0.04	0.04	0.04	0.04	0.04	0.04	0.04	0.04	0.04	0.04	0.04	0.04	0.04	0.04	0.04	0.04	0.04
0.03	0.01	0.00	0.01	0.05	0.01	0.01	0.03	0.02	0.02	0.07	0.06	0.01	0.06	0.00	0.00	0.05
0.04	0.04	0.04	0.04	0.04	0.04	0.04	0.04	0.04	0.04	0.04	0.04	0.04	0.04	0.04	0.04	0.04

Figure 16: Uncontrolled UO_2 assembly percent error of the capture density in the fuel rods and standard deviation of the percent error

Table 16: Distribution of uncontrolled UO_2 assembly tally results of the capture density in the fuel rods compared against a Gaussian distribution

	Capture Density (%)	Gaussian Distribution (%)
1 σ	70.4545455	68.2689492
2 σ	97.7272727	95.4499736
3 σ	100.0000000	99.7300203
4 σ	100.0000000	99.9936657
5 σ	100.0000000	99.9999426

0.03	0.00	0.00	0.01	0.00	0.00	0.00	0.03	0.00	0.01	0.01	0.00	0.00	0.00	0.01	0.02	0.01
0.01	0.01	0.01	0.01	0.01	0.01	0.01	0.01	0.01	0.01	0.01	0.01	0.01	0.01	0.01	0.01	0.01
0.01	0.00	0.01	0.01	0.00	0.01	0.01	0.00	0.01	0.01	0.01	0.01	0.01	0.01	0.01	0.03	0.02
0.01	0.01	0.01	0.01	0.01	0.01	0.01	0.01	0.01	0.01	0.01	0.01	0.01	0.01	0.01	0.01	0.01
0.00	0.00	0.01	0.01	0.01	0.00	0.01	0.00	0.00	0.02	0.00	0.00	0.01	0.03	0.01	0.01	0.00
0.01	0.01	0.01	0.01	0.01	0.01	0.01	0.01	0.01	0.01	0.01	0.01	0.01	0.01	0.01	0.01	0.01
0.00	0.00	0.00	0.02	0.00	0.00	0.01	0.00	0.03	0.01	0.00	0.00	0.01	0.01	0.01	0.01	0.01
0.01	0.01	0.01	0.01	0.01	0.01	0.01	0.01	0.01	0.01	0.01	0.01	0.01	0.01	0.01	0.01	0.01
0.01	0.01	0.02	0.00	0.01	0.01	0.00	0.01	0.01	0.01	0.01	0.02	0.02	0.01	0.02	0.02	0.00
0.01	0.01	0.01	0.01	0.01	0.01	0.01	0.01	0.01	0.01	0.01	0.01	0.01	0.01	0.01	0.01	0.01
0.02	0.00	0.01	0.01	0.02	0.00	0.00	0.01	0.01	0.02	0.02	0.04	0.02	0.00	0.00	0.00	0.00
0.01	0.01	0.01	0.01	0.01	0.01	0.01	0.01	0.01	0.01	0.01	0.01	0.01	0.01	0.01	0.01	0.01
0.02	0.00	0.01	0.02	0.02	0.02	0.01	0.01	0.01	0.01	0.01	0.02	0.01	0.01	0.01	0.01	0.02
0.01	0.01	0.01	0.01	0.01	0.01	0.01	0.01	0.01	0.01	0.01	0.01	0.01	0.01	0.01	0.01	0.01
0.01	0.01	0.01	0.02	0.01	0.01	0.01	0.02	0.00	0.00	0.02	0.01	0.02	0.01	0.02	0.04	0.03
0.01	0.01	0.01	0.01	0.01	0.01	0.01	0.01	0.01	0.01	0.01	0.01	0.01	0.01	0.01	0.01	0.01
0.01	0.01	0.02	0.00	0.01	0.01	0.02	0.01	0.00	0.02	0.02	0.01	0.02	0.01	0.02	0.03	0.07
0.01	0.01	0.01	0.01	0.01	0.01	0.01	0.01	0.01	0.01	0.01	0.01	0.01	0.01	0.01	0.01	0.01
0.02	0.01	0.01	0.02	0.01	0.02	0.01	0.01	0.00	0.01	0.02	0.03	0.02	0.02	0.00	0.04	0.05
0.01	0.01	0.01	0.01	0.01	0.01	0.01	0.01	0.01	0.01	0.01	0.01	0.01	0.01	0.01	0.01	0.01
0.04	0.02	0.01	0.02	0.03	0.04	0.03	0.02	0.01	0.01	0.00	0.01	0.00	0.01	0.01	0.04	0.05
0.01	0.01	0.01	0.01	0.01	0.01	0.01	0.01	0.01	0.01	0.01	0.01	0.01	0.01	0.01	0.01	0.01
0.01	0.02	0.03	0.02	0.04	0.02	0.02	0.02	0.03	0.00	0.01	0.00	0.01	0.00	0.01	0.01	0.04
0.01	0.01	0.01	0.01	0.01	0.01	0.01	0.01	0.01	0.01	0.01	0.01	0.01	0.01	0.01	0.01	0.01
0.02	0.00	0.02	0.02	0.01	0.00	0.01	0.02	0.02	0.03	0.00	0.00	0.01	0.01	0.02	0.03	0.04
0.01	0.01	0.01	0.01	0.01	0.01	0.01	0.01	0.01	0.01	0.01	0.01	0.01	0.01	0.01	0.01	0.01
0.01	0.01	0.00	0.01	0.01	0.00	0.02	0.02	0.00	0.00	0.00	0.01	0.00	0.01	0.02	0.01	0.04
0.01	0.01	0.01	0.01	0.01	0.01	0.01	0.01	0.01	0.01	0.01	0.01	0.01	0.01	0.01	0.01	0.01
0.01	0.01	0.01	0.00	0.03	0.02	0.01	0.01	0.01	0.02	0.03	0.01	0.01	0.03	0.02	0.02	0.05
0.01	0.01	0.01	0.01	0.01	0.01	0.01	0.01	0.01	0.01	0.01	0.01	0.01	0.01	0.01	0.01	0.01
0.01	0.00	0.00	0.00	0.02	0.00	0.01	0.01	0.00	0.00	0.00	0.01	0.00	0.02	0.02	0.03	0.04
0.01	0.01	0.01	0.01	0.01	0.01	0.01	0.01	0.01	0.01	0.01	0.01	0.01	0.01	0.01	0.01	0.01
0.01	0.00	0.01	0.01	0.03	0.01	0.01	0.01	0.00	0.03	0.01	0.00	0.01	0.01	0.02	0.04	0.02
0.01	0.01	0.01	0.01	0.01	0.01	0.01	0.01	0.01	0.01	0.01	0.01	0.01	0.01	0.01	0.01	0.01

Figure 17: Uncontrolled UO_2 assembly percent error of the moderator flux and standard deviation of the percent error

Table 17: Distribution of uncontrolled UO_2 assembly tally results of the moderator flux compared against a Gaussian distribution

	Moderator Flux (%)	Gaussian Distribution (%)
1 σ	65.0519031	68.2689492
2 σ	91.0034602	95.4499736
3 σ	97.9238754	99.7300203
4 σ	99.6539792	99.9936657
5 σ	100.0000000	99.9999426

Many of the conclusions here are the same as those reached in the uncontrolled UO_2 case. The locations of the percent errors are random and do not have any noticeable affect from boundary conditions or its location with respect to guide tubes. The locations of the maximum errors are in the same pins, but not necessarily in the same order from largest to smallest. The moderator flux uncertainties are lower than the density tally uncertainties because of the cross section error propagation taking place in the density tally results.

MOX

The results of the assembly eigenvalue are shown below in Table 18. The difference here is larger than those from the controlled and uncontrolled UO_2 case. This is because of the larger number of nuclides used in the MOX fuel pins that have unresolved resonance tables. Because the only differences between the two cross section sets are in these tables, there would be larger differences here than in either of the UO_2 assemblies.

Table 18: MOX assembly eigenvalue results

Cross Section Set	MCNP	MANE
K_∞	1.03339	1.03337
Standard Deviation (pcm)	2	2
Difference (pcm)	-	2

Total tally statistics are shown below in Table 19, and the energy-dependent moderator flux statistics are shown in Table 20. In addition, maps of the percent errors as well as the error in the percent errors for each of the tallies are shown in Figure 18-20. The coloring scheme from the controlled UO_2 case is employed in these figures as well. Tables 18-20, shown beneath these figures 18-20, shows the same statistical representations as in the controlled UO_2 case.

Table 19: MOX assembly total tally results

Tally	MAX & S.D. (%)	AVG (%)	RMS (%)	MRE (%)	UNC (%)
Fission Density	0.174 (0.057)	0.045	0.056	0.046	0.041
Capture Density	0.129 (0.057)	0.039	0.048	0.039	0.036
Moderator Flux	0.042 (0.014)	0.012	0.015	0.012	0.010

Table 20: MOX assembly energy dependent moderator flux results

Energy (MeV)	MAX & S.D. (%)	AVG (%)	RMS (%)	MRE (%)	UNC (%)
1.46E-07	0.285 (0.113)	0.070	0.089	0.070	0.068
6.25E-07	0.269 (0.071)	0.057	0.073	0.057	0.056
3.93E-06	0.222 (0.056)	0.049	0.062	0.048	0.042
1.30E-04	0.110 (0.042)	0.031	0.040	0.031	0.030
9.12E-03	0.081 (0.028)	0.026	0.032	0.026	0.022
8.21E-01	0.075 (0.028)	0.019	0.024	0.019	0.020
2.23E+00	0.110 (0.028)	0.030	0.038	0.030	0.023
2.00E+01	0.125 (0.042)	0.034	0.041	0.034	0.030

The average percent errors are larger than those from either the controlled UO_2 or the uncontrolled UO_2 cases. This is partly due to the MOX fuel pins containing more unique isotopes (9 in the MOX fuel pins, 3 in the UO_2 fuel pins), which would lead to a larger number of uncertainties in the cross sections, which leads to a higher tally uncertainty. Even with these higher uncertainties, the average percent errors agree with the uncertainties from the MCNP output. Another interesting phenomenon is the trend of the uncertainties in the energy-dependent moderator flux results. They decrease with increasing energies up until the last energy point, where it increases again. This is seen in all of the assembly-level cases, but is more pronounced in this MOX assembly. The cause of this trend is most likely due to the number of neutrons that interact in that energy range. More neutron interactions lead to a smaller uncertainty in the tally results.

0.03	0.02	0.05	0.01	0.05	0.05	0.01	0.08	0.06	0.02	0.10	0.04	0.02	0.04	0.02	0.01	0.00
0.07	0.07	0.07	0.07	0.06	0.06	0.06	0.06	0.06	0.06	0.06	0.06	0.06	0.07	0.07	0.07	0.07
0.05	0.04	0.01	0.07	0.02	0.04	0.00	0.03	0.02	0.01	0.01	0.07	0.08	0.09	0.05	0.13	0.03
0.07	0.06	0.06	0.06	0.06	0.06	0.06	0.06	0.06	0.06	0.06	0.06	0.06	0.06	0.06	0.06	0.07
0.08	0.10	0.01	0.02	0.10		0.03	0.02		0.02	0.12		0.03	0.07	0.02	0.07	0.02
0.07	0.06	0.06	0.06	0.06		0.06	0.06		0.06	0.06		0.06	0.06	0.06	0.06	0.07
0.04	0.06	0.08		0.08	0.03	0.02	0.03	0.01	0.04	0.05	0.04	0.04		0.06	0.01	0.03
0.07	0.06	0.06		0.06	0.06	0.06	0.06	0.06	0.06	0.06	0.06	0.06		0.06	0.06	0.07
0.02	0.06	0.14	0.07	0.00	0.00	0.02	0.04	0.04	0.02	0.02	0.01	0.02	0.02	0.02	0.09	0.02
0.06	0.06	0.06	0.06	0.06	0.06	0.06	0.06	0.06	0.06	0.06	0.06	0.06	0.06	0.06	0.06	0.06
0.06	0.06		0.02	0.12		0.03	0.02		0.05	0.02		0.01	0.00		0.00	0.14
0.06	0.06		0.06	0.06		0.06	0.06		0.06	0.06		0.06	0.06		0.06	0.06
0.05	0.07	0.07	0.03	0.02	0.11	0.01	0.01	0.10	0.02	0.15	0.06	0.17	0.04	0.08	0.03	0.03
0.06	0.06	0.06	0.06	0.06	0.06	0.06	0.06	0.06	0.06	0.06	0.06	0.06	0.06	0.06	0.06	0.06
0.01	0.00	0.04	0.07	0.02	0.01	0.00	0.12	0.06	0.03	0.02	0.02	0.04	0.01	0.02	0.06	0.00
0.06	0.06	0.06	0.06	0.06	0.06	0.06	0.06	0.06	0.06	0.06	0.06	0.06	0.06	0.06	0.06	0.06
0.04	0.02		0.06	0.05		0.04	0.03		0.07	0.05		0.06	0.05		0.02	0.06
0.06	0.06		0.06	0.06		0.06	0.06		0.06	0.06		0.06	0.06		0.06	0.06
0.03	0.06	0.04	0.09	0.12	0.03	0.01	0.02	0.09	0.04	0.03	0.06	0.01	0.11	0.10	0.01	0.04
0.06	0.06	0.06	0.06	0.06	0.06	0.06	0.06	0.06	0.06	0.06	0.06	0.06	0.06	0.06	0.06	0.06
0.03	0.09	0.03	0.01	0.09	0.02	0.04	0.02	0.06	0.10	0.05	0.01	0.06	0.06	0.02	0.02	0.04
0.06	0.06	0.06	0.06	0.06	0.06	0.06	0.06	0.06	0.06	0.06	0.06	0.06	0.06	0.06	0.06	0.06
0.06	0.03		0.07	0.03		0.03	0.05		0.07	0.02		0.02	0.03		0.01	0.10
0.06	0.06		0.06	0.06		0.06	0.06		0.06	0.06		0.06	0.06		0.06	0.06
0.06	0.01	0.04	0.10	0.08	0.06	0.06	0.02	0.03	0.00	0.07	0.00	0.04	0.01	0.00	0.13	0.11
0.06	0.06	0.06	0.06	0.06	0.06	0.06	0.06	0.06	0.06	0.06	0.06	0.06	0.06	0.06	0.06	0.06
0.03	0.10	0.06		0.04	0.16	0.06	0.01	0.07	0.07	0.02	0.04	0.04		0.06	0.08	0.01
0.07	0.06	0.06		0.06	0.06	0.06	0.06	0.06	0.06	0.06	0.06	0.06		0.06	0.06	0.07
0.02	0.04	0.08	0.02	0.09		0.10	0.02		0.02	0.10		0.04	0.02	0.09	0.05	0.06
0.07	0.06	0.06	0.06	0.06		0.06	0.06		0.06	0.06		0.06	0.06	0.06	0.06	0.07
0.06	0.01	0.11	0.03	0.08	0.01	0.05	0.03	0.03	0.06	0.02	0.04	0.03	0.01	0.04	0.01	0.04
0.07	0.06	0.06	0.06	0.06	0.06	0.06	0.06	0.06	0.06	0.06	0.06	0.06	0.06	0.06	0.06	0.07
0.04	0.02	0.08	0.05	0.03	0.08	0.05	0.01	0.08	0.03	0.02	0.01	0.01	0.07	0.03	0.03	0.06
0.07	0.07	0.07	0.07	0.06	0.06	0.06	0.06	0.06	0.06	0.06	0.06	0.06	0.07	0.07	0.07	0.07

Figure 18: MOX assembly percent error of the fission density in the fuel rods and standard deviation of the percent error

Table 21: Distribution of MOX assembly tally results of the fission density in the fuel rods compared against a Gaussian distribution

	Fission Density (%)	Gaussian Distribution (%)
1 σ	70.0757576	68.2689492
2 σ	95.8333333	95.4499736
3 σ	99.6212121	99.7300203
4 σ	100.0000000	99.9936657
5 σ	100.0000000	99.9999426

0.03	0.03	0.04	0.07	0.12	0.00	0.03	0.04	0.00	0.06	0.10	0.06	0.04	0.07	0.10	0.01	0.04
0.06	0.06	0.06	0.06	0.06	0.06	0.06	0.06	0.06	0.06	0.06	0.06	0.06	0.06	0.06	0.06	0.06
0.06	0.07	0.03	0.11	0.00	0.02	0.03	0.03	0.05	0.02	0.04	0.08	0.05	0.06	0.08	0.13	0.00
0.06	0.06	0.06	0.06	0.06	0.04	0.06	0.06	0.04	0.06	0.06	0.04	0.06	0.06	0.06	0.06	0.06
0.07	0.09	0.04	0.01	0.08		0.04	0.04		0.02	0.08		0.05	0.08	0.01	0.06	0.01
0.06	0.06	0.06	0.04	0.04		0.04	0.04		0.04	0.04		0.04	0.04	0.06	0.06	0.06
0.03	0.07	0.03		0.00	0.00	0.06	0.02	0.07	0.01	0.03	0.02	0.03		0.09	0.04	0.02
0.06	0.06	0.04		0.04	0.04	0.04	0.04	0.04	0.04	0.04	0.04	0.04		0.04	0.06	0.06
0.05	0.04	0.09	0.07	0.03	0.05	0.02	0.03	0.01	0.01	0.04	0.03	0.06	0.04	0.02	0.03	0.04
0.06	0.06	0.04	0.04	0.04	0.04	0.06	0.06	0.04	0.06	0.06	0.04	0.04	0.04	0.04	0.06	0.06
0.08	0.02		0.04	0.09		0.02	0.03		0.05	0.04		0.04	0.01		0.04	0.11
0.06	0.04		0.04	0.04		0.04	0.04		0.04	0.04		0.04	0.04		0.04	0.06
0.01	0.04	0.09	0.03	0.03	0.03	0.01	0.01	0.06	0.01	0.09	0.08	0.10	0.01	0.05	0.01	0.03
0.06	0.06	0.04	0.04	0.06	0.04	0.06	0.06	0.04	0.06	0.06	0.04	0.06	0.04	0.04	0.06	0.06
0.02	0.05	0.05	0.09	0.02	0.02	0.01	0.09	0.02	0.05	0.02	0.04	0.02	0.01	0.05	0.03	0.03
0.06	0.06	0.04	0.04	0.06	0.04	0.06	0.06	0.04	0.06	0.06	0.04	0.06	0.04	0.04	0.06	0.06
0.02	0.07		0.06	0.02		0.03	0.05		0.01	0.06		0.00	0.02		0.02	0.00
0.06	0.04		0.04	0.04		0.04	0.04		0.04	0.04		0.04	0.04		0.04	0.06
0.05	0.01	0.01	0.04	0.04	0.00	0.02	0.04	0.10	0.07	0.01	0.01	0.04	0.03	0.08	0.01	0.04
0.06	0.06	0.04	0.04	0.06	0.04	0.06	0.06	0.04	0.06	0.06	0.04	0.06	0.04	0.04	0.06	0.06
0.01	0.06	0.01	0.02	0.03	0.01	0.02	0.00	0.05	0.07	0.03	0.04	0.05	0.06	0.03	0.04	0.01
0.06	0.06	0.04	0.04	0.06	0.04	0.06	0.06	0.04	0.06	0.06	0.04	0.06	0.04	0.04	0.06	0.06
0.03	0.01		0.03	0.02		0.00	0.01		0.04	0.03		0.02	0.05		0.03	0.09
0.06	0.04		0.04	0.04		0.04	0.04		0.04	0.04		0.04	0.04		0.04	0.06
0.02	0.04	0.03	0.05	0.09	0.01	0.06	0.01	0.07	0.02	0.02	0.08	0.04	0.03	0.00	0.06	0.06
0.06	0.06	0.04	0.04	0.04	0.04	0.06	0.06	0.04	0.06	0.06	0.04	0.04	0.04	0.04	0.06	0.06
0.02	0.04	0.09		0.00	0.12	0.01	0.02	0.05	0.04	0.03	0.02	0.03		0.04	0.02	0.00
0.06	0.06	0.04		0.04	0.04	0.04	0.04	0.04	0.04	0.04	0.04	0.04		0.04	0.06	0.06
0.01	0.03	0.07	0.00	0.08		0.09	0.10		0.01	0.08		0.05	0.01	0.10	0.04	0.01
0.06	0.06	0.06	0.04	0.04		0.04	0.04		0.04	0.04		0.04	0.04	0.06	0.06	0.06
0.01	0.01	0.08	0.02	0.02	0.05	0.01	0.02	0.03	0.06	0.01	0.03	0.04	0.03	0.08	0.02	0.03
0.06	0.06	0.06	0.06	0.06	0.04	0.06	0.06	0.04	0.06	0.06	0.04	0.06	0.06	0.06	0.06	0.06
0.02	0.01	0.09	0.08	0.00	0.05	0.01	0.00	0.01	0.03	0.01	0.05	0.03	0.04	0.08	0.03	0.01
0.06	0.06	0.06	0.06	0.06	0.06	0.06	0.06	0.06	0.06	0.06	0.06	0.06	0.06	0.06	0.06	0.06

Figure 19: MOX assembly percent error of the capture density in the fuel rods and standard deviation of the percent error

Table 22: Distribution of MOX assembly tally results of the capture density in the fuel rods compared against a Gaussian distribution

	Capture Density (%)	Gaussian Distribution (%)
1 σ	69.3181818	68.2689492
2 σ	94.6969697	95.4499736
3 σ	100.0000000	99.7300203
4 σ	100.0000000	99.9936657
5 σ	100.0000000	99.9999426

0.02	0.04	0.00	0.03	0.02	0.01	0.01	0.04	0.02	0.01	0.00	0.00	0.00	0.01	0.01	0.03	0.00
0.03	0.01	0.01	0.01	0.01	0.01	0.01	0.01	0.01	0.01	0.01	0.01	0.01	0.01	0.01	0.01	0.03
0.00	0.02	0.03	0.03	0.01	0.00	0.01	0.01	0.03	0.02	0.02	0.01	0.01	0.01	0.02	0.00	0.01
0.01	0.01	0.01	0.01	0.01	0.01	0.01	0.01	0.01	0.01	0.01	0.01	0.01	0.01	0.01	0.01	0.01
0.01	0.02	0.01	0.00	0.00	0.02	0.00	0.00	0.02	0.02	0.01	0.01	0.01	0.00	0.00	0.00	0.01
0.01	0.01	0.01	0.01	0.01	0.01	0.01	0.01	0.01	0.01	0.01	0.01	0.01	0.01	0.01	0.01	0.01
0.01	0.01	0.02	0.01	0.01	0.00	0.01	0.01	0.01	0.01	0.01	0.00	0.03	0.00	0.02	0.01	0.02
0.01	0.01	0.01	0.01	0.01	0.01	0.01	0.01	0.01	0.01	0.01	0.01	0.01	0.01	0.01	0.01	0.01
0.02	0.00	0.02	0.01	0.00	0.00	0.02	0.01	0.02	0.01	0.01	0.02	0.00	0.00	0.01	0.01	0.00
0.01	0.01	0.01	0.01	0.01	0.01	0.01	0.01	0.01	0.01	0.01	0.01	0.01	0.01	0.01	0.01	0.01
0.03	0.02	0.02	0.01	0.02	0.01	0.02	0.00	0.01	0.00	0.01	0.03	0.02	0.01	0.01	0.02	0.00
0.01	0.01	0.01	0.01	0.01	0.01	0.01	0.01	0.01	0.01	0.01	0.01	0.01	0.01	0.01	0.01	0.01
0.01	0.02	0.02	0.01	0.00	0.01	0.01	0.01	0.01	0.02	0.00	0.00	0.02	0.00	0.00	0.01	0.01
0.01	0.01	0.01	0.01	0.01	0.01	0.01	0.01	0.01	0.01	0.01	0.01	0.01	0.01	0.01	0.01	0.01
0.01	0.00	0.03	0.02	0.02	0.02	0.00	0.02	0.00	0.00	0.01	0.00	0.00	0.01	0.01	0.02	0.00
0.01	0.01	0.01	0.01	0.01	0.01	0.01	0.01	0.01	0.01	0.01	0.01	0.01	0.01	0.01	0.01	0.01
0.02	0.01	0.03	0.04	0.01	0.01	0.01	0.00	0.01	0.00	0.01	0.01	0.02	0.01	0.00	0.01	0.00
0.01	0.01	0.01	0.01	0.01	0.01	0.01	0.01	0.01	0.01	0.01	0.01	0.01	0.01	0.01	0.01	0.01
0.00	0.01	0.01	0.02	0.03	0.00	0.00	0.02	0.01	0.01	0.00	0.02	0.01	0.02	0.02	0.01	0.00
0.01	0.01	0.01	0.01	0.01	0.01	0.01	0.01	0.01	0.01	0.01	0.01	0.01	0.01	0.01	0.01	0.01
0.02	0.01	0.01	0.00	0.01	0.01	0.01	0.00	0.01	0.01	0.01	0.00	0.02	0.01	0.00	0.00	0.01
0.01	0.01	0.01	0.01	0.01	0.01	0.01	0.01	0.01	0.01	0.01	0.01	0.01	0.01	0.01	0.01	0.01
0.00	0.00	0.00	0.02	0.00	0.02	0.00	0.00	0.02	0.01	0.01	0.01	0.01	0.01	0.01	0.02	0.00
0.01	0.01	0.01	0.01	0.01	0.01	0.01	0.01	0.01	0.01	0.01	0.01	0.01	0.01	0.01	0.01	0.01
0.01	0.00	0.01	0.02	0.01	0.01	0.01	0.00	0.01	0.01	0.01	0.00	0.03	0.02	0.02	0.01	0.00
0.01	0.01	0.01	0.01	0.01	0.01	0.01	0.01	0.01	0.01	0.01	0.01	0.01	0.01	0.01	0.01	0.01
0.01	0.01	0.01	0.01	0.01	0.00	0.02	0.03	0.02	0.01	0.02	0.02	0.03	0.01	0.01	0.00	0.01
0.01	0.01	0.01	0.01	0.01	0.01	0.01	0.01	0.01	0.01	0.01	0.01	0.01	0.01	0.01	0.01	0.01
0.02	0.02	0.04	0.03	0.01	0.03	0.02	0.02	0.00	0.00	0.01	0.00	0.00	0.01	0.02	0.01	0.00
0.01	0.01	0.01	0.01	0.01	0.01	0.01	0.01	0.01	0.01	0.01	0.01	0.01	0.01	0.01	0.01	0.01
0.01	0.02	0.01	0.01	0.02	0.01	0.02	0.02	0.01	0.04	0.03	0.02	0.00	0.01	0.03	0.00	0.02
0.01	0.01	0.01	0.01	0.01	0.01	0.01	0.01	0.01	0.01	0.01	0.01	0.01	0.01	0.01	0.01	0.01
0.00	0.01	0.01	0.01	0.00	0.00	0.01	0.02	0.03	0.04	0.01	0.00	0.02	0.01	0.04	0.01	0.00
0.03	0.01	0.01	0.01	0.01	0.01	0.01	0.01	0.01	0.01	0.01	0.01	0.01	0.01	0.01	0.01	0.03

Figure 20: MOX assembly percent error of the moderator flux and standard deviation of the percent error

Table 23: Distribution of MOX assembly tally results of the moderator flux compared against a Gaussian distribution

	Moderator Flux (%)	Gaussian Distribution (%)
1 σ	65.3979239	68.2689492
2 σ	94.8096886	95.4499736
3 σ	100.0000000	99.7300203
4 σ	100.0000000	99.9936657
5 σ	100.0000000	99.9999426

Again, many of the conclusions here are the same as those reached in the uncontrolled UO_2 case and the controlled UO_2 case. The locations of the percent errors are random and do not have any noticeable affect from boundary conditions or its location with respect to guide tubes. The locations of the maximum errors are in the same pins, but not necessarily in the same order from largest to smallest. The moderator flux uncertainties are lower than the density tally uncertainties because of the cross section error propagation taking place in the density tally results.

Whole Core

The results of the whole core eigenvalue are shown below in Table 24. The results here are in very good agreement, which could be a cause for concern since the MOX assemblies were off by 2 pcm. The results here agree so well partly due to the agreement of the cross sections, but also due to some error cancelation of the errors present in the MOX assemblies.

Table 24: Whole core eigenvalue results

Cross Section Set	MCNP	MANE
K_∞	1.00698	1.00699
Standard Deviation (pcm)	2	2
Difference (pcm)	-	1

The pin fission densities and energy-dependent flux in the moderator were also tallied in 4 representative assemblies as described in chapter 3. The fission density tally statistics are shown below in Table 25, and the total flux in the moderator tally statistics are shown below in Table 26.

Table 25: Whole core fission density tally results

Tally	MAX & S.D. (%)	AVG (%)	RMS (%)	MRE (%)	UNC (%)
Full MOX	1.084 (0.336)	0.284	0.358	0.284	0.239
Half MOX	1.192 (0.448)	0.291	0.356	0.291	0.225
Diagonal UO2	0.766 (0.243)	0.226	0.293	0.222	0.173
Half Controlled UO2	1.603 (0.654)	0.344	0.447	0.339	0.296

Table 26: Whole core total moderator flux tally results

Tally	MAX & S.D. (%)	AVG (%)	RMS (%)	MRE (%)	UNC (%)
Full MOX	0.226 (0.085)	0.064	0.082	0.064	0.060
Half MOX	0.314 (0.099)	0.080	0.101	0.081	0.058
Diagonal UO2	0.276 (0.071)	0.080	0.099	0.080	0.057
Half Controlled UO2	0.441 (0.127)	0.130	0.160	0.130	0.090

Once again, the average percent errors are either less than or only slightly greater than the uncertainty from the MCNP output file. The average percent errors here are larger than the uncertainty confirming there is some error cancelation occurring in the eigenvalue results shown in table 23 above. In addition, each of the same statistical tests was used on each of the energy groups for the flux in the moderator. These results are shown below in Tables 27-30.

Table 27: Whole core tally results for energy dependent moderator flux of the full MOX assembly

Energy (MeV)	MAX & S.D. (%)	AVG (%)	RMS (%)	MRE (%)	UNC (%)
1.46E-07	1.906 (0.590)	0.410	0.517	0.393	0.359
6.25E-07	1.336 (0.447)	0.352	0.438	0.343	0.308
3.93E-06	1.132 (0.336)	0.274	0.350	0.275	0.238
1.30E-04	0.569 (0.211)	0.178	0.222	0.177	0.159
9.12E-03	0.587 (0.169)	0.150	0.192	0.148	0.129
8.21E-01	0.379 (0.127)	0.109	0.138	0.108	0.092
2.23E+00	0.533 (0.199)	0.139	0.176	0.139	0.136
2.00E+01	0.784 (0.242)	0.192	0.241	0.191	0.161

Table 28: Whole core tally results for energy dependent moderator flux of the half MOX assembly

Energy (MeV)	MAX & S.D. (%)	AVG (%)	RMS (%)	MRE (%)	UNC (%)
1.46E-07	1.528 (0.431)	0.364	0.484	0.353	0.343
6.25E-07	1.608 (0.612)	0.317	0.395	0.314	0.293
3.93E-06	1.321 (0.475)	0.278	0.345	0.278	0.226
1.30E-04	0.650 (0.225)	0.166	0.204	0.167	0.151
9.12E-03	0.658 (0.242)	0.155	0.192	0.155	0.123
8.21E-01	0.443 (0.169)	0.125	0.155	0.126	0.088
2.23E+00	0.566 (0.239)	0.172	0.209	0.172	0.131
2.00E+01	0.719 (0.281)	0.171	0.220	0.170	0.155

Table 29: Whole core tally results for energy dependent moderator flux of the diagonal uncontrolled UO_2 assembly

Energy (MeV)	MAX & S.D. (%)	AVG (%)	RMS (%)	MRE (%)	UNC (%)
1.46E-07	1.210 (0.517)	0.279	0.360	0.265	0.213
6.25E-07	0.738 (0.267)	0.228	0.282	0.230	0.205
3.93E-06	0.835 (0.295)	0.203	0.266	0.202	0.205
1.30E-04	0.562 (0.284)	0.171	0.213	0.172	0.148
9.12E-03	0.558 (0.239)	0.150	0.190	0.150	0.124
8.21E-01	0.331 (0.127)	0.100	0.123	0.100	0.092
2.23E+00	0.588 (0.249)	0.150	0.187	0.151	0.135
2.00E+01	0.645 (0.214)	0.213	0.259	0.214	0.160

Table 30: Whole core tally results for energy dependent moderator flux of the half controlled UO_2 assembly

Energy (MeV)	MAX & S.D. (%)	AVG (%)	RMS (%)	MRE (%)	UNC (%)
1.46E-07	2.779 (0.832)	0.566	0.712	0.549	0.439
6.25E-07	1.638 (0.835)	0.427	0.544	0.418	0.394
3.93E-06	1.558 (0.459)	0.379	0.477	0.367	0.357
1.30E-04	0.850 (0.414)	0.271	0.334	0.269	0.240
9.12E-03	0.654 (0.271)	0.207	0.267	0.208	0.189
8.21E-01	0.726 (0.281)	0.164	0.210	0.163	0.137
2.23E+00	0.809 (0.281)	0.242	0.297	0.241	0.211
2.00E+01	1.164 (0.559)	0.308	0.386	0.305	0.252

The uncertainty decreases as energy increases through 2.23 MeV, just like the assembly cases. The average percent errors here are, again, all slightly larger than the uncertainties, but not by a large enough value to be cause for concern. The differences in the uncertainties between these tallies are due to the location of the assemblies in the core. The half MOX and diagonal uncontrolled UO_2 assemblies are located closer to the center of the core where the number of neutrons would be the greatest, meaning the uncertainties would be smaller in those assemblies. The full MOX and controlled UO_2 assemblies were located farther away from the center, meaning the magnitude of the flux there would be less than the magnitude at the center where the other two assemblies are located. This would lead to a larger uncertainty in the full MOX and controlled UO_2 assemblies.

CHAPTER 5

CONCLUSION AND FUTURE WORK

In this work, the utilization code MANE was created to run NJOY99 to process ENDF format cross sections into the ACE file format. These cross sections were shown to be in exact agreement with the cross sections provided by MCNP, with the exception of some small round off errors (on the order of 10^{-6}) and the unresolved resonance tables. Those differences were due to machine precision differences and the random number generator called by NJOY at the beginning of the unresolved resonance cross section calculations, respectively. Cross sections generated by MANE were used for five MCNP verification runs to calculate the eigenvalue and several tally densities. In each of these runs, the eigenvalues were found to be within 10 pcm with one another, and the tallies were found to be on the order of 0.1% different when compared to the stochastic uncertainties of those tallies as calculated by MCNP.

The largest source of error was the differences found in the unresolved resonance region tables. The errors could be resolved by changing variables in the PURR input. There are several different variables that could be changed in the PURR input, such as the number of probability bins (currently set at 20). Another variable to change would be the number of resonance ladders (currently set to 64), which sets how many samples are taken before an average cross section for that particular probability bin is determined.

APPENDIX A

MATERIAL SPECIFICATIONS

Material Number Densities (10^24 atoms)								
Material	MOX (4.3%)	MOX (7.0%)	MOX (8.7%)	UO2	Moderator	Center Tube	Control	Clad
Temperature (K)	1200	1200	1200	1200	600	600	600	900 (fuel rod) 600 (other)
U-235	5.00E-05	5.00E-05	5.00E-05	8.65E-04		1.00E-08		
U-238	2.21E-02	2.21E-02	2.21E-02	2.23E-02				
Pu-238	1.50E-05	2.40E-05	3.00E-05					
Pu-239	5.80E-04	9.30E-04	1.16E-03					
Pu-240	2.40E-04	3.90E-04	4.90E-04					
Pu-241	9.80E-05	1.52E-04	1.90E-04					
Pu-242	5.40E-05	8.40E-05	1.05E-04					
Am-241	1.30E-05	2.00E-05	2.50E-05					
O-16	4.63E-02	4.63E-02	4.63E-02	4.62E-02	2.44E-02	2.44E-02		
H-1					4.89E-02	4.89E-02		
B-10					2.32E-05	2.32E-05	1.60E-02	
B-11					9.34E-05	9.34E-05	6.43E-02	
C-12							2.01E-02	
Zr-90								2.21E-02
Zr-91								4.82E-03
Zr-92								7.35E-03
Zr-94								7.48E-03
Zr-96								1.20E-03

REFERENCES

[1] MacFarlane, R.E., 1999. NJOY-99 nuclear data processing system. <http://t2.lanl.gov/codes/njoy99/index.html>.

[2] F.B. Brown, et al., "MCNP Versino 5," *Trans. Am. Nucl. Soc.*, **87**, pp. 273-276 (November, 2002).

[3] Forrest B. Brown, "The makxsf Code with Doppler Broadening", LA-UR-06-7002 (2006).

[4] A.C. Kahler III, R. MacFarlane, "The NJOY Nuclear Data Processing System, Version 2012", LA-UR-12-27079 (2012)

[5] H. Trellue, R. Little, M.B. Lee, "New ACE-Formatted Neutron and Proton Libraries Based on ENDF/B-VII.0", LA-UR-08-1999 (2008).

[6] H. Trellue, R. Little, "Release of New MCNP S(α,β) Library ENDF70SAB Based on ENDF/B-VII.0", LA-UR-08-3628 (2008).

[7] M.Mattes and J.Keinert, "Thermal Neutron Scattering Data for the Moderator Materials H2O, D2O, and ZrHx in ENDF-6 Format and as ACE Library for MCNP(X) Codes," INDC/NDS report INDC(NDS)-0470 (April 2005).

[8] R.E. MacFarlane, "New Thermal Neutron Scattering Files for ENDF/B-VI Release 2", LA-12639-MS (March 1994).

[9] F. Rahnema, R. Hon, S. Douglass, "A Stylized Three-Dimensional Pressurized Water Reactor Benchmark Problem With UO_2 And MOX Fuel." *Nuclear Technology* 184.1 (2013): 1-28.